

1 **Biomass burning influence on high latitude tropospheric ozone and reactive**  
2 **nitrogen in summer 2008: a multi-model analysis based on POLMIP**  
3 **simulations.**

4 S.R. Arnold<sup>1\*</sup>, L.K. Emmons<sup>2</sup>, S.A. Monks<sup>1</sup>, K.S. Law<sup>3</sup>, D.A. Ridley<sup>4</sup>, S. Turquety<sup>5</sup>, S. Tilmes<sup>2</sup>, J.L.  
5 Thomas<sup>3</sup>, I. Bouarar<sup>3</sup>, J. Flemming<sup>6</sup>, V. Huijnen<sup>7</sup>, J. Mao<sup>8</sup>, B.N. Duncan<sup>9</sup>, S. Steenrod<sup>9</sup>, Y. Yoshida<sup>9</sup>, J.  
6 Langner<sup>10</sup>, Y. Long<sup>5</sup>

- 7
- 8 1. Institute for Climate and Atmospheric Science, School of Earth & Environment, University of Leeds, UK.
  - 9 2. Atmospheric Chemistry Division, NCAR, USA.
  - 10 3. UPMC Univ. Paris 06; Université Versailles St-Quentin; CNRS/INSU; UMR 8190, Paris, France.
  - 11 4. Department of Civil and Environmental Engineering, Massachusetts Institute of Technology, Cambridge,  
12 MA, USA.
  - 13 5. Laboratoire de Météorologie Dynamique, IPSL, CNRS, UMR8539, 91128 Palaiseau Cedex, France.
  - 14 6. ECMWF, Reading, UK.
  - 15 7. Royal Netherlands Meteorological Institute (KNMI), De Bilt, The Netherlands.
  - 16 8. Program in Atmospheric and Oceanic Sciences, Princeton University and Geophysical Fluid Dynamics  
17 Laboratory/National Oceanic and Atmospheric Administration, Princeton, New Jersey, USA.
  - 18 9. NASA Goddard Space Flight Center, Greenbelt, MD, USA.
  - 19 10. Swedish Meteorological and Hydrological Institute, 60176 Norrköping, Sweden.

20  
21  
22 \*Correspondence to: [s.arnold@leeds.ac.uk](mailto:s.arnold@leeds.ac.uk)

23  
24  
25  
26  
27

28 **Abstract**

29 We have evaluated tropospheric ozone enhancement in air dominated by biomass burning  
30 emissions at high latitudes ( $> 50^{\circ}\text{N}$ ) in July 2008, using 10 global chemical transport model  
31 simulations from the POLMIP multi-model comparison exercise. In model air masses dominated by  
32 fire emissions,  $\Delta\text{O}_3/\Delta\text{CO}$  values ranged between 0.039 and 0.196 ppbv/ppbv (mean: 0.113  
33 ppbv/ppbv) in freshly fire-influenced air, and between 0.140 and 0.261 ppbv/ppbv (mean: 0.193  
34 ppbv) in more aged fire-influenced air. These values are in broad agreement with the range of  
35 observational estimates from the literature. Model  $\Delta\text{PAN}/\Delta\text{CO}$  enhancement ratios show distinct  
36 groupings according to the meteorological data used to drive the models. ECMWF-forced models  
37 produce larger  $\Delta\text{PAN}/\Delta\text{CO}$  values (4.47 to 7.00 pptv/ppbv) than GEOS5-forced models (1.87 to 3.28  
38 pptv/ppbv), which we show is likely linked to differences in efficiency of vertical transport during  
39 poleward export from mid-latitude source regions. Simulations of a large plume of biomass burning  
40 and anthropogenic emissions exported from towards the Arctic using a Lagrangian chemical  
41 transport model show that 4-day net ozone change in the plume is sensitive to differences in plume  
42 chemical composition and plume vertical position among the POLMIP models. In particular, Arctic  
43 ozone evolution in the plume is highly sensitive to initial concentrations of PAN, as well as  
44 oxygenated VOCs (acetone, acetaldehyde), due to their role in producing the peroxyacetyl radical  
45 PAN precursor. Vertical displacement is also important due to its effects on the stability of PAN, and  
46 subsequent effect on  $\text{NO}_x$  abundance. In plumes where net ozone production is limited, we find that  
47 the lifetime of ozone in the plume is sensitive to hydrogen peroxide loading, due to the production  
48 of  $\text{HO}_2$  from peroxide photolysis, and the key role of  $\text{HO}_2 + \text{O}_3$  in controlling ozone loss. Overall, our  
49 results suggest that emissions from biomass burning lead to large-scale photochemical  
50 enhancement in high latitude tropospheric ozone during summer.

51

52 **1. Introduction**

53 Vegetation fires play an important role in ecosystem function and regulation (Bonan, 2008) and  
54 contribute substantially to atmospheric CO<sub>2</sub>, with gross emissions from biomass burning estimated  
55 to be between 2 and 4 PgC a<sup>-1</sup> globally, equivalent to 40% of those from fossil fuel combustion (Ciais  
56 et al., 2013). Biomass burning also impacts atmospheric chemistry, releasing large quantities of  
57 aerosol and reactive gas-phase chemical compounds, including CO, NO<sub>x</sub> (=NO+NO<sub>2</sub>) and volatile  
58 organic compounds (VOCs) (Andreae et al., 1988; van der Werf et al., 2010). These emissions result  
59 in perturbations to tropospheric oxidants, aerosol loading and the atmospheric radiative balance  
60 (Dentener et al., 2006). Studies have demonstrated that wildfires in the boreal regions of North  
61 America and Eurasia affect abundances of atmospheric trace gases and aerosol at high latitudes  
62 (Bourgeois and Bey, 2011; Fisher et al., 2010; Hornbrook et al., 2011; Jaffe and Wigder, 2012; Monks  
63 et al., 2012; Paris et al., 2009; Real et al., 2007; Warneke et al., 2010; Wofsy et al., 1992). These  
64 contributions peak during spring and summer, when large fires occur naturally in the regions of  
65 Alaska and Canada and in central and eastern Siberia (Monks et al., 2012; van der Werf et al., 2010).  
66 How anthropogenic and natural sources of climatically-relevant atmospheric constituents will  
67 contribute to future high latitude climate change is highly uncertain (Shindell et al., 2008). In  
68 particular, our understanding of how boreal fires impact large-scale Arctic and high latitude budgets  
69 of climate-relevant atmospheric constituents is limited, and is reliant on sparse observations, often  
70 in specific events and isolated plumes. Short-lived climate pollutants (SLCPs) such as tropospheric  
71 ozone, aerosol and methane may contribute to accelerated rates of warming observed in the Arctic  
72 relative to the global mean temperature increase (Quinn et al., 2008). Changes in tropospheric  
73 ozone and aerosol may already have contributed 0.2–0.4°C and 0.5–1.4°C respectively to Arctic  
74 surface warming since 1890 (Shindell and Faluvegi, 2009). A better understanding of boreal fire  
75 influence on high latitude tropospheric ozone and aerosol is essential for improving the reliability of  
76 our projections of future Arctic and northern hemisphere climate change, especially considering  
77 proposed climate-fire feedbacks which may enhance the intensity and extent of high latitude  
78 wildfire under a warming climate (de Groot et al., 2013).

79 The role of boreal fires as a source of high latitude tropospheric ozone is particularly poorly  
80 constrained, and has been the subject of some controversy, with different studies suggesting both  
81 minor and major roles for fires as a source of Arctic ozone. A recent review by (Jaffe and Wigder,  
82 2012) showed that most studies have demonstrated net production of tropospheric ozone from  
83 wildfire emissions, due to the propensity of fires to emit large quantities of key ozone precursors  
84 (NO<sub>x</sub>, CO, VOCs). The  $\Delta O_3/\Delta CO$  enhancement ratio (defined as the excess ozone mixing ratio above  
85 background ozone in an air mass normalized by an enhancement in CO mixing ratio above

86 background CO), is often used as a measure of ozone production efficiency in fire plumes as they are  
87 processed downwind from emission. Values of  $\Delta\text{O}_3/\Delta\text{CO}$  in boreal wildfire plumes from Siberia,  
88 Alaska and Canada vary between approximately  $-0.1 \text{ ppbv ppbv}^{-1}$  and  $0.6 \text{ ppbv ppbv}^{-1}$  (Alvarado et  
89 al., 2010; Bertschi et al., 2004; Goode et al., 2000; Honrath et al., 2004; Martin et al., 2006;  
90 Mauzerall et al., 1996; Paris et al., 2009; Parrington et al., 2013; Pfister et al., 2006; Real et al., 2007;  
91 Singh et al., 2010; Tanimoto et al., 2008; Wofsy et al., 1992). In addition, these values are observed  
92 to generally increase with increasing plume age.

93 A robust estimate of the role of boreal fires in producing tropospheric ozone is hampered by a large  
94 range in observational estimates of ozone production efficiency, likely resulting from factors such as  
95 variability in emission factors with combustion efficiency and vegetation type, differences in plume  
96 age, different plume chemical processing, due to e.g. different aerosol loadings, and mixing with  
97 anthropogenic emissions (Jaffe and Wigder, 2012). Integrated analysis of data from multiple boreal  
98 fire plumes sampled across Alaska and Canada during the ARCTAS-B campaign concluded that boreal  
99 fire emissions had only negligible impact on tropospheric ozone profiles in summer 2008 over Alaska  
100 and Canada (Alvarado et al., 2010; Singh et al., 2010). However, plumes sampled were mostly freshly  
101 emitted ( $< 2$  days), and box modelling based on the same data suggests high in-situ photochemical  
102 production rates, despite little to no measured ozone enhancement in these plumes (Olson et al.,  
103 2012). Other recent modelling studies have suggested greater ozone sensitivity to boreal fire  
104 emissions in more aged air masses. Tropospheric ozone in coastal Canada has been shown to be  
105 highly sensitive to NO<sub>x</sub> emissions from central Canadian fires (Parrington et al., 2012), and regional  
106 modelling for the Arctic in summer 2008 suggests that ozone production increases markedly in fire  
107 plumes downwind from emission as air masses process chemically over time (Thomas et al., 2013).  
108 Wespes et al., (2012), using a tagged NO<sub>x</sub> and ozone production scheme in the MOZART-4 global  
109 CTM, showed that more than 20% of ozone in the Arctic lower troposphere is produced from NO<sub>x</sub>  
110 emitted from high latitude fires in North America and Asia. Boreal forest fires have also been shown  
111 to be an important source of peroxyacetyl nitrate (PAN) in the Arctic during the spring and summer  
112 months (Jacob et al., 1992; Singh et al., 2010; Singh et al., 1992). Transport of PAN from lower  
113 latitudes into the Arctic makes a substantial contribution to local in-situ ozone production, via NO<sub>2</sub>  
114 released from PAN decomposition (Walker et al., 2012).

115 In light of uncertainties associated with these contributions, there is a need to better evaluate how  
116 models simulate the influence of boreal fires on high latitude budgets of ozone and precursors,  
117 particularly in summer, when local radiative processes play a major role in Arctic surface  
118 temperatures (Shindell, 2007). While several model studies have investigated simulated ozone  
119 production from boreal fires, there has been little attempt to understand how differences in model

120 treatments of chemistry and transport affect estimates of ozone production in fire-influenced air  
121 masses.

122 In this paper, we use results from POLMIP (POLARCAT model intercomparison Project) (Emmons et  
123 al., 2014) and observations collected in the Arctic troposphere as part of the ARCTAS-B mission  
124 (Jacob et al., 2010), to evaluate simulated summertime tropospheric ozone and its precursors in the  
125 northern high latitudes and how it is influenced by boreal fire emissions in a series of state-of-the-art  
126 global atmospheric chemical transport models. The POLMIP model experiments and observations  
127 used to evaluate them are described in Section 2. In Section 3, we use idealised model tracers to  
128 track fire emissions, and compare ozone enhancement ratios ( $\Delta O_3/\Delta CO$ ) in air dominated by fire  
129 emission influence across the range of models, and investigate relationships with model NO<sub>y</sub>  
130 partitioning. Section 4 describes a case study of a large biomass burning plume exported from  
131 Siberia in July 2008, which we use to investigate the sensitivities of Arctic tropospheric ozone to  
132 model chemistry based on Lagrangian chemical model simulations of the plume. Our findings and  
133 conclusions are summarised in Section 5.

134

## 135 **2. Model simulations and observations**

136 The POLARCAT Model Intercomparison Project (POLMIP) was designed to evaluate the performance  
137 of several global and regional-scale chemical transport models (CTMs) in the Arctic troposphere  
138 (Emmons et al., 2014). POLMIP contributes to the POLARCAT project aim to better understand  
139 model deficiencies identified in a previous evaluation of CTM simulations of Arctic tropospheric  
140 ozone and its precursors, and aims to exploit the large amount of observational data collected  
141 during the IPY aircraft experiments in the Arctic troposphere during spring and summer 2008.  
142 Further details on the POLARCAT project and the 2008 aircraft campaigns are given in Law et al.,  
143 (2014). All models used the same data for emissions, with the aim of allowing an investigation of  
144 model differences due to atmospheric transport and chemical processes only. The exception was the  
145 GEOS-Chem model, which used different anthropogenic emissions (Emmons et al., 2014). POLMIP  
146 anthropogenic emissions are those provided for the ARCTAS project by D. Streets (Argonne National  
147 Lab) and University of Iowa (<http://bio.cgrer.uiowa.edu/arctas/emission.html>). Daily biomass  
148 burning emissions are taken from the Fire Inventory of NCAR (FINN), based on MODIS fire counts  
149 (Wiedinmyer et al., 2011). All POLMIP models injected biomass burning emissions into the lowest  
150 boundary layer model level, in order to remove any differences produced through treatments of fire  
151 emission injection heights. Other emissions (biogenic, ocean, volcano) were derived from the  
152 MACCity inventory (Lamarque et al., 2010). Table 1 summarises details of the POLMIP model

153 simulations used in this study. Further details of the POLMIP model experiments, emissions data and  
154 evaluation of the simulations can be found in Emmons et al., (2014).

155 The GEOS-Chem model includes a parameterization for transition metal-catalysed formation of H<sub>2</sub>O  
156 from aerosol uptake of HO<sub>2</sub>, rather than formation of H<sub>2</sub>O<sub>2</sub>. This process is effectively an irreversible  
157 loss for HO<sub>x</sub>, and is motivated by the suggestion from field observations that HO<sub>2</sub> uptake to aerosol  
158 may not produce H<sub>2</sub>O<sub>2</sub>. This motivation and the implementation of this scheme are described by  
159 Mao et al., (2013b). The same study showed that inclusion of this process reduces the mass-  
160 weighted global mean OH concentration by 12%, and substantially increases CO concentrations at  
161 high latitudes due to an increased CO lifetime. It was also shown to reduce surface ozone by 3-10  
162 ppbv over North America and Eurasia.

163 To further aid in understanding inter-model differences in transport, POLMIP models included fixed  
164 lifetime tracers from anthropogenic and biomass burning emission sources. A total of 6 tracers were  
165 simulated, each with a prescribed fixed atmospheric lifetime of 25 days. A 25-day tracer lifetime is  
166 sufficiently long relative to the transport timescale for long-range transport from mid-latitudes to  
167 the Arctic (days to a week), while being short enough to avoid the formation of a homogeneous well-  
168 mixed tracer distribution. Two tracers were emitted from each of three mid-latitude continental  
169 source regions (Europe, North America and Asia), one with the same source as the anthropogenic CO  
170 emissions and one from the CO emissions from biomass burning sources. Details on the exact  
171 definition of source regions and emission magnitudes are given in Emmons et al., (2014). The Asian  
172 biomass burning tracer is dominated by emissions from large Siberian fires in July 2008 (see Emmons  
173 et al., 2014). Monks et al. (2012) demonstrated that variability in emissions from boreal fires  
174 dominates the inter-annual variability of the ozone precursor, CO in the Arctic troposphere. Using  
175 fixed-lifetime CO tracers from the POLMIP simulations, Monks et al., (2014) used these tracers in  
176 conjunction with observed and simulated CO to investigate the contributions from differences in  
177 model transport and oxidants to inter-model variability in simulated seasonal CO in the Arctic. They  
178 showed that emissions from Asian fires are the dominant source of CO tracer in the lower and  
179 middle Arctic troposphere, and are approximately equal to the contribution from Asian  
180 anthropogenic sources in the upper troposphere. Here, we exploit these tracers to identify regions  
181 and periods in the POLMIP model simulations for which air is strongly influenced by fire emissions.

182 Several aircraft flew missions into the Arctic troposphere during summer 2008 as part of the  
183 POLARCAT experiment (Law et al., 2014). The POLARCAT-France and GRACE experiments, based in  
184 south-west Greenland sampled aged fire plumes and anthropogenic air masses transported into the  
185 Arctic from Siberia and North America. ARCTAS-B, based in central Canada, sampled fresh and aged

186 fire emissions over Canada and the Arctic. In this analysis, we make use only of data from the  
187 ARCTAS-B mission, for which the NASA DC8 aircraft was equipped with an extensive suite of gas  
188 phase and aerosol instrumentation, including ozone, CO, speciated oxides of nitrogen (NO<sub>y</sub>), volatile  
189 organic compounds and peroxides (Jacob et al., 2010). Monks et al., (2014) present a detailed  
190 comparison of the POLMIP model simulations with CO and ozone data from all POLARCAT  
191 experiments.

192 During ARCTAS-B, the DC8 aircraft made 7 flights, based from Cold Lake, Canada from 29th June to  
193 10th July 2008. The vast majority of observations were made in fresh Saskatchewan fire plumes,  
194 although some flights also targetted aged plumes transported to Canada from Siberian and  
195 Californian fires. All ARCTAS DC8 data are available in a publicly accessible archive ([http://www-  
196 air.larc.nasa.gov/cgi-bin/arcstat-c](http://www-air.larc.nasa.gov/cgi-bin/arcstat-c)), and described in Jacob et al., (2010).

197

### 198 **3. Fire emission influence on ozone and NO<sub>y</sub> enhancement in POLMIP models**

#### 199 **3.1 Evaluation of model ozone and ozone precursors in air dominated by fire emissions**

200 Using the fixed-lifetime tracers from the models, we evaluate simulations of ozone and precursors  
201 against ARCTAS-B aircraft observations in air dominated by fire emissions in the summertime Arctic  
202 troposphere. Figures 1-4 respectively show aircraft observations of ozone, CO, PAN and HNO<sub>3</sub>  
203 plotted against hourly model output interpolated in time and space to the aircraft position. For each  
204 model, points have been coloured according to whether the simulated tracers from fire sources or  
205 from anthropogenic sources contribute more than 50% of the total (fire + anthropogenic) tracer  
206 mixing ratio at the aircraft location. In model air dominated by fire emissions, simulated ozone  
207 generally falls close to the observation-model 1:1 line, and model median biases vary between -22%  
208 and +5%, compared with -19% to -2% in anthropogenic-dominated air. As discussed in detail by  
209 Monks et al., (2014), all POLMIP models display a negative CO bias, throughout the depth of the  
210 troposphere. Use of the POLMIP fixed-lifetime tracers shows that this is the case in both  
211 anthropogenic and fire-dominated air. Global models typically underestimate CO in the northern  
212 extratropics. A recent multi-model study showed negative annual mean model biases exceeding -45  
213 ppbv compared with surface CO observations at high latitudes, and as large as -30 ppbv compared  
214 with satellite- retrieved CO concentrations at 500 hPa over the extra-tropical oceans (Naik et al,  
215 2013). The majority of ARCTAS-B observations were made in fresh biomass burning plumes, leading  
216 to larger CO concentrations on average in fire-dominated air masses. The models also simulate  
217 larger CO concentrations in these air masses, but with a general underestimate. Monks et al., (2014)

218 demonstrated that POLMIP model-simulated global mean OH was generally biased slightly high  
219 compared with observational constraints, possibly contributing to their low CO bias.

220 Simulated distributions of NO<sub>y</sub> species show some of the largest diversity between models and  
221 largest fractional biases against observations. Emmons et al., (2014) showed that POLMIP models  
222 display large variability in their budgets of NO<sub>y</sub> throughout the depth of the Arctic troposphere. The  
223 POLMIP models fall into two distinct groups in terms of their simulation of ARCTAS-B PAN  
224 concentrations. Models forced by GEOS5 meteorology tend to have lower PAN than observed in fire-  
225 dominated air (median biases: -47% to -28%), while the ECMWF-forced models produce PAN  
226 concentrations close to or larger than those observed in fire-dominated air (median biases: -2% to  
227 +24%). This major difference appears to be related to differences in the efficiency of vertical  
228 transport between models using the two different sets of meteorological data (see Section 3.3).  
229 Models that transport PAN and its precursors more rapidly to higher altitudes and lower  
230 temperatures will likely promote enhanced PAN formation and stability (Singh and Hanst, 1981).  
231 These effects on differences in NO<sub>y</sub> partitioning are explored further in Section 3.3.

232 GEOS-Chem underestimates DC8 PAN concentrations by the largest magnitude overall (median bias -  
233 51%), with lower-than-observed PAN at all locations where observed PAN exceeds 250 pptv. Recent  
234 work has substantially improved the simulation of PAN in the GEOS-Chem model (Fischer et al.,  
235 2014), however these model updates are not included here. The CIFS model shows very large PAN  
236 overestimates (> factor of 4) in fire air masses sampled close to the surface. Comparisons with  
237 aircraft observations (see Emmons et al., 2014) show coincident overestimates in NO<sub>2</sub> and  
238 acetaldehyde, suggesting these very large PAN concentrations may be partly produced by  
239 overestimates in PAN precursors near to fire source regions. In general, the models display  
240 substantially larger range in PAN biases in fire-dominated air (median biases: -47% to +24%)  
241 compared with anthropogenic-dominated air (median biases: -34% to +5%). Fresh biomass burning  
242 plumes observed in ARCTAS-B displayed enhancements in peroxyacetyl precursors such as  
243 acetaldehyde and acetone (Hornbrook et al., 2011). Simulated oxygenated (o)VOC enhancements  
244 relative to CO (particularly for acetone) in the POLMIP models show large variability close to  
245 Canadian fires (Emmons et al., 2014), which may in turn lead to a large range in simulated PAN  
246 production. With the exception of the GEOS-Chem and TM5 models, emissions of acetone and  
247 acetaldehyde are the same for all models. The large diversity in model concentrations of these  
248 species therefore mainly results from different treatments of organic chemistry, differences in rates  
249 of photochemical processing of their parent VOCs and differences in their photolysis and OH loss.

250 Several models show a large positive bias in Arctic HNO<sub>3</sub> concentrations (up to a factor 32 in  
251 anthropogenically-dominated air). In an earlier study, Alvarado et al. (2010) used the GEOS-Chem  
252 model to study HNO<sub>3</sub> in fire-influenced air masses. This study concluded that the over-prediction of  
253 HNO<sub>3</sub> was due to under-prediction of NO<sub>x</sub> conversion to PAN in fire Influenced air masses. The  
254 POLMIP models do not generally support this offsetting of positive biases in HNO<sub>3</sub> with under-  
255 prediction of PAN.

### 256 **3.2 Model ozone production in fire-dominated Arctic air masses**

257 Previous studies have directly determined the contribution from fire emissions to model ozone by  
258 removing emissions from fires (Pfister et al., 2006; Thomas et al., 2013) or by chemically tagging  
259 ozone produced by NO<sub>x</sub> emitted from fires (Wespes et al., 2012). To investigate this contribution in  
260 the POLMIP models, we use the 25-day fixed-lifetime tracers to identify the dominant emission  
261 source that influences high latitude air in the models. We calculate enhancement in tropospheric  
262 ozone as a ratio to CO enhancement ( $\Delta O_3/\Delta CO$ ) where the fixed-lifetime tracers indicate that the  
263 model domain is dominated by fire emissions. Points are considered to be fire-dominated where the  
264 fire-sourced fixed-lifetime tracer concentration is at least 66% of the total fixed lifetime tracer  
265 concentration, and where the fire-sourced fixed-lifetime tracer mixing ratio is at least 10 ppbv. Using  
266 this minimum tracer mixing ratio to define air enhanced in fire emissions, we use the slope of CO vs  
267 ozone in these air masses to calculate the  $\Delta O_3/\Delta CO$  ratio directly. This avoids the definition of a CO  
268 mixing ratio enhancement above background CO, which due to OH differences between the models  
269 is highly model dependent (Monks et al., 2014).

270 Recent studies have highlighted the need for caution regarding the use of O<sub>3</sub>/CO slopes to diagnose  
271 photochemical ozone production, particularly in remote regions, due to slopes being artificially  
272 increased by chemical loss of CO due to reaction with OH (e.g. Voulgarakis et al., 2011; Zhang et al.,  
273 2014). Chemical rate output from the MOZART-4 model shows that in the domain of our study  
274 (latitude 50N-90N, 850-250 hPa) the daily chemical loss rate of CO is small (average 1.9 ppbv/day),  
275 equivalent to 1.5%-4.5%. This loss is partly offset by chemical production of CO from VOC oxidation  
276 (average 0.9 ppbv/day), and daily fractional rates of chemical ozone production at the same  
277 locations are substantially larger (~5 - 45%). This analysis suggests that chemical CO loss is unlikely to  
278 have a significant effect on our calculated ozone/CO slopes.

279 Using changes in the ratio of concentrations of two co-emitted VOCs with differing atmospheric  
280 lifetimes, it is also possible to estimate how model  $\Delta O_3/\Delta CO$  values change, as air dominated by fire  
281 emissions is transported away from the source region and ages photochemically. For primary-  
282 emitted VOCs that have losses dominated by OH-oxidation, the concentration ratio of a more

283 reactive to a less reactive VOC is expected to reduce over time since emission (Calvert, 1976).  
284 Propane ( $C_3H_8$ ) and ethane ( $C_2H_6$ ) have respective atmospheric e-folding lifetimes of approximately 5  
285 and 24 days (for an average OH concentration of  $2 \times 10^6$  molec/cm<sup>3</sup> (Atkinson et al., 2006)). In the  
286 absence of mixing with background concentrations, a decrease in the  $\ln([C_3H_8]/[C_2H_6])$  ratio is  
287 directly proportional to the time elapsed since emission.

288 We use the  $\ln([C_3H_8]/[C_2H_6])$  ratios from the POLMIP models to create relationships between broad  
289 classifications of air mass age and  $\Delta O_3/\Delta CO$ . Based on model values of the  $\ln([C_3H_8]/[C_2H_6])$  ratio, we  
290 separate the distribution of high latitude tropospheric model grid boxes into two populations of  
291 ‘youngest’ (points with  $\ln([C_3H_8]/[C_2H_6])$  values larger than the mean) and ‘oldest’ (points with  
292  $\ln([C_3H_8]/[C_2H_6])$  values smaller than the mean) air masses, in terms of their estimated age since  
293 emission. Figure 5 shows POLMIP model-simulated relationships between  $[O_3]$  and  $[CO]$  in fire-  
294 dominated air in the high latitude free troposphere (latitude > 50N; 850 hPa > pressure > 250 hPa),  
295 with calculated  $\Delta O_3/\Delta CO$  slopes in youngest and oldest air mass groups as defined by the  
296  $\ln([C_3H_8]/[C_2H_6])$  ratios. The SMHI-MATCH and GEOS-Chem models respectively did not explicitly  
297 simulate propane and the fixed-lifetime source tracers. Therefore, it is not possible to calculate  
298  $\Delta O_3/\Delta CO$  slopes in fire-dominated air according to these age classes.

299 POLMIP model  $\Delta O_3/\Delta CO$  slopes are positive in both the younger and aged fire-dominated air in all  
300 models. Slopes in the aged air masses (mean: 0.193 , min: 0.140, max: 0.261 ppbv/ppbv) are larger  
301 on average compared with slopes in the younger air masses (mean: 0.113 , min: 0.039, max: 0.196  
302 ppbv/ppbv). This is indicative of photochemical ozone production in fire emission-dominated air  
303 emitted into and advected to high latitudes in the POLMIP models, with an increase in ozone  
304 enhancement relative to CO enhancement in these air masses as they age photochemically. Two  
305 models (TOMCAT and CAM5-Chem) show a slight decrease in  $\Delta O_3/\Delta CO$  with air mass age defined by  
306 the  $\ln([C_3H_8]/[C_2H_6])$  ratio. Supplementary Fig. S1 shows that the  $\ln([\text{propane}]/[\text{ethane}])$  ratio for  
307 these models show less distinct separation in their corresponding fire tracer concentrations between  
308 the ‘young’ and ‘old’ age classes. This suggests that the  $\ln([C_3H_8]/[C_2H_6])$  ratio may be a less robust  
309 proxy for photochemical age since emission in these models. Figure 5k shows ozone and CO  
310 observations from ARCTAS-B DC8 flights over-plotted with  $\Delta O_3/\Delta CO$  slopes from the different  
311 POLMIP models. Although the DC8 aircraft sampled only a small proportion of the fire-dominated  
312 domain simulated by the models, the aircraft points lie close to the model  $\Delta O_3/\Delta CO$  slopes.  
313 Observed ozone concentrations appear slightly larger as a function of CO than those in the POLMIP  
314 simulations. There is also evidence that observed air masses show a larger range in ozone  
315 enhancements for a given range of CO enhancement than those simulated, perhaps reflecting a  
316 diverse range of fresh plumes sampled by the aircraft close to the fires on the model sub-grid scale.

317 POLMIP model  $\Delta O_3/\Delta CO$  values are highly consistent compared with the wide range of  $\Delta O_3/\Delta CO$   
318 values determined from observational studies in boreal fire plumes. Figure 6 compares the  $\Delta O_3/\Delta CO$   
319 values from the POLMIP models with  $\Delta O_3/\Delta CO$  values from previous model and observational  
320 studies on fire plumes at high latitudes. Average  $\Delta O_3/\Delta CO$  values from a previous GEOS-Chem model  
321 study based on ARCTAS-B range between -0.07 and 0.01 (Alvarado et al., 2010), substantially smaller  
322 than values from the POLMIP models. Moreover, these values indicate a tendency for ozone loss in  
323 fire plumes, however these values were diagnosed in freshly fire-influenced air masses. The POLMIP  
324 models agree well with regional WRF-chem model simulations for the ARCTAS-B campaign, which  
325 produced mean  $\Delta O_3/\Delta CO$  values in fresh and aged biomass burning plumes of 0.08 and 0.49  
326 ppbv/ppbv respectively, and used the same FINN fire emissions as the POLMIP models (Thomas et  
327 al., 2013). Differences in simulated photolysis between the POLMIP models are likely contributors to  
328 model spread in photochemical ozone enhancement relative to CO. Such differences are presented  
329 and explored for the POLMIP models by Emmons et al., (2014). Mao et al., (2013a), using the GFDL  
330 AM3 model with aerosol loss uptake of  $HO_2$ , characterized a suppressed large-scale ozone  
331 enhancement from fires ( $\Delta O_3/\Delta CO = 0.16$ ) at high latitudes ( $> 60N$ ) compared with the tropics. This is  
332 also seen in comparisons of observational studies between different latitudes, however observed  
333  $\Delta O_3/\Delta CO$  at high latitudes is often larger than this large-scale average value derived from their  
334 model (Jaffe and Wigder, 2012). Both heterogeneous  $HO_2$  loss on aerosol (Mao et al., 2013) and  
335 bromine chemistry (Parrella et al., 2012), implemented in GEOS-Chem for POLMIP may also play a  
336 role in reducing tropospheric ozone abundance.

337 Overlaying  $O_3/CO$  slopes from the other POLMIP models onto plots of GEOS-Chem and SMHI-MATCH  
338  $[O_3]$  vs  $[CO]$  allows some comparison of their efficiency of Arctic tropospheric  $[O_3]$  production with  
339 other POLMIP models. POLMIP model  $O_3/CO$  slopes lie through the  $[O_3]$  vs  $[CO]$  distribution from the  
340 SMHI-MATCH model, which at larger  $[CO]$ , shows a slope value consistent with the smaller slope  
341 values from other POLMIP models. GEOS-Chem shows the lowest ozone enhancement as a function  
342 of CO among the POLMIP models, outside of the range of the majority of other models and the  
343 ARCTAS-B observations.

344

### 345 **3.3 High latitude PAN enhancement in POLMIP models**

346 Enhancements in PAN relative to CO in the high latitude troposphere in the POLMIP models show  
347 grouping according to the source of meteorological data used to drive the models. Analogous to the  
348 ozone enhancement ratio ( $\Delta O_3/\Delta CO$ ),  $\Delta PAN/\Delta CO$  can be used to evaluate the efficiency of PAN  
349 formation and its transport to high latitudes in the POLMIP models (Fig. 7). Observations show that

350 PAN was the dominant NO<sub>y</sub> component in the Arctic troposphere during summer 2008 (Alvarado et  
351 al., 2010; Liang et al., 2011), and as a source of NO<sub>x</sub>, may be an important driver of tropospheric  
352 ozone production at high latitudes (Walker et al., 2012). Average  $\Delta$ PAN/ $\Delta$ CO values in GEOS5-forced  
353 models range between 1.87-3.28 pptv/ppbv, and in ECMWF-forced models range between 4.47-7.00  
354 pptv/ppbv. Along with the biases shown in Fig. 3, this further suggests that major differences in  
355 summertime NO<sub>y</sub> partitioning may be driven by differences in model vertical transport efficiency.  
356 While differences in PAN abundances in the Arctic troposphere shown in Fig. 3 could be explained by  
357 differences in efficiency of poleward pollution transport in the models generally, differences in  
358  $\Delta$ PAN/ $\Delta$ CO slopes reflect inter-model variability in the efficiency of PAN production or transport  
359 relative to CO. CO has a long atmospheric lifetime relative to the transport timescales characteristic  
360 of poleward frontal export, and is dominated by primary emissions. Therefore,  $\Delta$ PAN/ $\Delta$ CO variability  
361 likely represents differences in the rate of PAN formation and its stability. This may be driven by  
362 different efficiencies of air mass uplift during boundary layer export, promoting PAN stability, or  
363 differences in organic chemistry, controlling the abundance of the acetyl peroxy radical precursor.

364 The vertical distributions of the 25-day fixed-lifetime CO tracers in the models indicate a more  
365 vertically well-mixed lower troposphere in the ECMWF models compared with the GEOS-5 models in  
366 general. Figure 8 shows zonal mean differences in tracers between 900hPa and 500hPa at northern  
367 hemisphere mid-latitudes in spring and summer. In spring, TOMCAT, TM5 and CIFS show a weaker  
368 vertical tracer gradient than CAM4-Chem, CAM5-Chem, MOZART-4 and GMI, suggesting less  
369 efficient vertical transport in the GEOS5-driven models over mid-latitude source regions. This  
370 pattern is less clear in summer, however between 45 and 55°N this general behaviour is evident  
371 among the same models, with the exception of MOZART-4, which becomes more vertically well-  
372 mixed. Mid-latitude convection is likely more important for vertical transport in summer. Increased  
373 convective vertical mixing in the models may therefore mask some of the differences in vertical  
374 tracer structure produced by differences in large-scale vertical transport.

375 Average values of  $\Delta$ PAN/ $\Delta$ CO from a range of fresh and aged fire plumes sampled during ARCTAS-B  
376 varied between 2.8 and 0.35 pptv/ppbv (Alvarado et al., 2010), in better agreement with values  
377 produced by the GEOS5-driven models. Figure 7k shows PAN and CO from ARCTAS-B observations.  
378 Observed PAN / CO slopes are broadly consistent with those simulated by the POLMIP models. The  
379 majority of observations support larger slopes consistent with the ECMWF-driven models. The  
380 largest PAN enhancements are produced by the CIFS model, which also shows the largest overall  
381 positive bias (+40%) against high latitude PAN observations (Fig. 3). Three POLMIP models use  
382 identical chemistry schemes (MOZART-4, CAM4-Chem, CAM5Chem). Among these three models,

383  $\Delta$ PAN/ $\Delta$ CO values increase from 1.91 to 3.55 pptv/ppbv, and  $\Delta$ O<sub>3</sub>/ $\Delta$ CO enhancements increase with  
384 this increasing Arctic PAN import efficiency. Across all POLMIP models, we see no robust relationship  
385 between increased Arctic PAN import efficiency and increased ozone production efficiency  
386 ( $\Delta$ O<sub>3</sub>/ $\Delta$ CO). Differences in photochemistry between the models likely determine the efficiency with  
387 which NO<sub>y</sub> import is manifested in high latitude ozone enhancement. In addition, a reduction in NO<sub>x</sub>  
388 through more rapid PAN formation in the ECMWF models, and consequent suppression of ozone  
389 production in plumes transported poleward may also play a role (Jacob et al., 1992; Mauzerall et al.,  
390 1996).

391 The NO<sub>y</sub> biases shown by GEOS-Chem are consistent with those shown in Alvarado et al. (2010),  
392 who found that PAN and HNO<sub>3</sub> in the GEOS-Chem model were under- and over-estimated  
393 respectively by almost a factor 2. In particular, the large negative bias in high latitude PAN (Fig. 3)  
394 may explain the lower ozone enhancement compared with other POLMIP models. This bias is largest  
395 among the POLMIP models. The simulated low PAN abundances are unlikely explained by the  
396 composition of emissions, since all POLMIP models use the same fire emissions.

#### 397 **4. Arctic fire plume sensitivities to model chemistry**

398 In order to further investigate the sensitivities of high latitude tropospheric ozone production to  
399 differences in POLMIP model NO<sub>y</sub> partitioning and photochemistry in fire plumes, we analyse  
400 chemical processing during the export of a large plume of Siberian biomass burning and  
401 anthropogenic emissions from Asia to the Arctic. By carrying out additional simulations using a  
402 Lagrangian chemical transport model, we quantify how differences in chemical composition of this  
403 plume between the POLMIP models following export from Asia and poleward transport, and  
404 differences in subsequent transport in the Arctic, impact the evolution of ozone in the plume.

#### 405 **4.1 Siberian biomass burning & Asian anthropogenic plume case study**

406 Between 6th and 9th July 2008, a low-pressure system travelled from Siberia across the Arctic Ocean  
407 towards the North Pole, carrying with it smoke plumes from Siberian wildfires and emissions from  
408 anthropogenic sources in East Asia. This extensive plume of polluted air was sampled both remotely  
409 from satellite and by aircraft in-situ measurements. The IASI (Infrared Atmospheric Sounding  
410 Interferometer) satellite instrument observed the plume as a large feature of enhanced CO that was  
411 exported from the Asian east coast and advanced towards the North Pole (Pommier et al., 2010). On  
412 6 and 7 July the plume was between 850 km and 1600 km wide, large enough to be represented on  
413 the grid-scale of the POLMIP global models. As part of ARCTAS-B, the DC8 aircraft also sampled the  
414 plume on 9<sup>th</sup> July, between 80 and 85°N, to the north of Greenland. Despite excessive diffusion in  
415 the polar region due to the singularity at the pole on the Eulerian global grid, Sodemann et al.,

416 (2011) showed that the TOMCAT global model was able to capture the large-scale export of the  
417 plume, its horizontal position, and its poleward transport into the Arctic region. This event provides  
418 a good case study for evaluation of differences in transport and chemistry of fire-influenced  
419 pollution to the Arctic among the POLMIP models.

420

421 The general horizontal position, size and shape of the plume agree well between the different  
422 POLMIP model simulations. This is likely due to the use of the same emissions data in each model,  
423 and large-scale horizontal flow associated with the low pressure system being largely consistent  
424 between different driving meteorological data. Figure 9 shows total column CO from the POLMIP  
425 models at 06:00UT on 7<sup>th</sup> July 2008, just as the leading edge of the plume reaches 80°N, at ~180°W.  
426 The plume extent and position simulated by the POLMIP models is also consistent with the observed  
427 IASI satellite CO columns (Sodemann et al., 2011). The positions and relative enhancement of  
428 simulated column CO maxima are controlled by simulated horizontal transport and diffusive  
429 processes at the sub-plume scale, but also vertical transport processes which control the export CO  
430 from the boundary layer and the extent to which exported pollution layers remain distinct or  
431 become vertically diffusive.

432

433 There are large differences in the magnitude of CO simulated in the plume. Differences in model OH  
434 have been shown to have a strong influence on inter-model variability in Arctic CO in the POLMIP  
435 models (Monks et al., 2014). These same differences are evident in Fig. 9, particularly in CO column  
436 differences in Arctic background air surrounding the plume enhancements. Figures 10 and 11 show  
437 column distributions of 25-day lifetime tracers emitted from Asian anthropogenic and Asian fire  
438 sources respectively. The lower resolution models tend to simulate more diffuse and poleward  
439 penetration of anthropogenic-emitted tracer into the Arctic compared with the CIFS model.

440

441 Although the plume appears as a largely coherent single feature in total column CO, the fixed-  
442 lifetime tracers reveal large-scale separation of anthropogenic and fire contributions. The leading  
443 edge of the plume in all models is dominated by fire emissions, with the main part of the  
444 anthropogenically-sourced air mass further to the south (Fig. 10). Backward modelling simulations  
445 with the FLEXPART Lagrangian particle dispersion model have also demonstrated that when this  
446 plume was sampled by the DC8 aircraft on 9<sup>th</sup> July 2008, CO contributions from anthropogenic and  
447 fire sources showed large-scale separation, with Asian fossil fuel sourced CO dominating above 6-  
448 7km altitude (Sodemann et al., 2011). Enhanced CO from the anthropogenic part of this plume was  
449 transported into the lowermost stratosphere, and was sampled by the DLR Falcon aircraft during the

450 POLARCAT-GRACE campaign on 10<sup>th</sup> July 2008 (Roiger et al., 2011). The separation between  
451 anthropogenic and fire influence within the plume is highly consistent across the POLMIP models,  
452 suggesting good agreement in the locations of export and large-scale horizontal transport of  
453 emissions from these two sources from the Asian boundary layer to the Arctic. The GMI and  
454 MOZART-4 model plume maxima are situated at lower altitudes compared to the other models  
455 (Table 2), again consistent with less efficient vertical export in GEOS5-driven models (Fig. 8).

456

#### 457 **4.2 Lagrangian chemical model simulations**

458 From each of the POLMIP global model simulations, the positions of plume maxima are determined  
459 from the plume distributions shown in Fig. 9. Maxima locations are determined by locating the  
460 model grid that contains the maximum Asian fire tracer mixing ratio in the horizontal and vertical in  
461 the region of the simulated plume. Table 2 shows the longitude, latitude and pressure of plume  
462 maxima in the POLMIP models at 06:00UT on 7<sup>th</sup> July 2008, following export from the Asian  
463 continental boundary layer and import into the Arctic. Table 2 also shows POLMIP model  
464 concentrations of key species for ozone photochemistry at these maxima locations. From these  
465 maxima locations in each POLMIP model, Lagrangian forward air mass trajectories are calculated  
466 using the ROTRAJ (Reading Offline Trajectory) Lagrangian transport model (Methven et al., 2003).  
467 Kinematic forward-trajectories from the plume maxima locations are calculated by integration of  
468 velocity fields taken from operational analyses of the European Centre for Medium-range Weather  
469 Forecasts (ECMWF). The fields at the Lagrangian particle positions are obtained from the 1.0125<sup>o</sup>  
470 horizontal resolution analyses by cubic Lagrange interpolation in the vertical followed by bilinear  
471 interpolation in the horizontal and linear interpolation in time. Five-day forward-trajectories were  
472 calculated with position output every 6 h. These trajectories account for large-scale advection by the  
473 resolved model winds, and neglect convective and turbulent transport.

474

475 Using initial chemical conditions from Table 2, and following the forward trajectories calculated from  
476 the plume maxima locations for each POLMIP model, we carry out Lagrangian chemical box model  
477 simulations using the CiTTYCAT (Cambridge Tropospheric Trajectory model of Chemistry and  
478 Transport) Lagrangian CTM (Pugh et al., 2012). The aim of these simulations is to test the sensitivity  
479 of ozone in the plume to differences in the chemical composition and the vertical position of the  
480 plume following import into the Arctic. Using the same Lagrangian model, Real et al. (2007)  
481 simulated photochemistry in an Alaskan biomass burning plume advected over the North Atlantic  
482 Ocean and sampled sequentially by several research aircraft. The model was able to reproduce the  
483 observed ozone change in the plume observed between aircraft interceptions. We use the CiTTYCAT

484 model in single box mode, with a chemical timestep of 5 minutes and physical conditions taken from  
485 the ECMWF trajectory data (position, temperature, specific humidity) updated every 30 minutes.  
486 Photochemical kinetic data is updated with information where available from the JPL  
487 recommendation (Sander et al., 2011), with further data from IUPAC (Atkinson et al., 2004, 2006;  
488 Crowley et al., 2010) and the Leeds Master Chemical Mechanism (<http://mcm.leeds.ac.uk>). In the  
489 absence of adequate observations of aerosol size distribution in the plume, we specify fixed aerosol  
490 surface area based on observed aerosol size distributions in the boreal fire plume analysed by Real  
491 et al. (2007). This surface area ( $3.0 \times 10^{-6} \text{ cm}^2/\text{cm}^3$ ) is used to calculate rates of heterogeneous  
492 chemistry in the CiTTYCAT plume simulations. In order to isolate sensitivities to chemical  
493 composition of the plume, we use a single chemistry scheme in the CiTTYCAT Lagrangian simulations  
494 (Pugh et al., 2012), and a single set of meteorological data (ECMWF operational analyses data) to  
495 calculate transport of the plume forward from 06:00UT on 7<sup>th</sup> July 2008.

496

#### 497 **4.3 Simulated plume ozone change and sensitivities to transport and chemistry**

498

499 We investigate the range of plume ozone production and loss rates produced by the diversity in  
500 chemical initial conditions and forward transport from the plume maxima positions in the POLMIP  
501 models. Figure 12a shows simulated 4-day ozone change from the CiTTYCAT model in the plume  
502 when initialised by different POLMIP model chemical conditions and when following individual  
503 forward trajectories from plume maxima locations. The 4-day evolution of pressure along each of  
504 these trajectories is shown in Fig. 12d. The 4-day ozone change differs by  $\sim 2.5$  ppbv across the range  
505 of POLMIP model initial concentrations and forward trajectories, with some models showing near-  
506 zero net ozone change (TM5, LMDZ-INCA), while others show net ozone loss of more than 2 ppbv  
507 (CAM4-Chem, CAM5-Chem). These differences are produced both by differences in the chemical  
508 composition of the plume and different transport pathways forwards over the 4 day period. In  
509 particular, differences in plume altitude and subsequent vertical displacement over the 4 days  
510 affects the formation and stability of PAN, as well as the balance between ozone production and loss  
511 via the reactions of  $\text{O}(^1\text{D})$  with water vapour and of  $\text{O}_3 + \text{HO}_2$ .

512 All plume simulations result in net ozone loss over 4 days, with ozone destruction dominated by the  
513 reaction of  $\text{O}_3 + \text{HO}_2$ . The TM5-initialised plume shows very little net ozone change, likely due to its  
514 relatively high altitude, suppressing both ozone production due to PAN stability and ozone loss due  
515 to the dry upper tropospheric conditions of the Arctic. The GMI-initialised plume shows a large  
516 ozone production tendency of  $2 \text{ ppbv day}^{-1}$  on average, which is balanced by large ozone loss rates  
517 of slightly larger but similar magnitude. Larger ozone production tendency is driven by the larger

518 NO<sub>x</sub> concentrations in this plume compared to those initialized from the other POLMIP models.  
519 Similar strong NO<sub>x</sub>-limitation of ozone production in Arctic biomass burning plumes was first noted  
520 during flights made in western Alaska during the ABLE3A mission (Jacob et al., 1992). The cycle of  
521 ozone production and loss rates in this simulation also suggests that the pathway followed by this  
522 plume from its initial position favours more efficient photochemistry, due to exposure to relatively  
523 more hours of peak solar radiation.

524 The simulated ozone change shows strong sensitivity to the physical position and displacement of  
525 the air mass forward trajectories. Figure 13 shows net changes in ozone and PAN from analogous  
526 CiTTYCAT simulations in which forward trajectories from each of the 7 model plume locations have  
527 been used in conjunction with the 7 sets of chemical initial conditions from the POLMIP models. This  
528 produces an ensemble of 49 Lagrangian model simulations, with varying combinations of chemical  
529 composition and physical displacement. This diversity produces a much larger range in ozone change  
530 over 4 days (approx.. -5 ppbv to +4 ppbv). Several simulations initialised by chemical conditions from  
531 the TOMCAT and GMI models result in net ozone production. These models have plume  
532 compositions enhanced in NO<sub>x</sub> and PAN compared with the other POLMIP models (Table 2). In  
533 particular, the conversion of enhanced PAN from the TOMCAT initial state to NO<sub>x</sub> (Fig. 13b) results  
534 in enhanced ozone production in forward trajectories that descend (LMDZ-INCA, MOZART-4) or  
535 begin at lower altitudes (GMI) (Fig. 12d).

536 Additional plume simulations using the CiTTYCAT model and the model-specific forward trajectories,  
537 reveal strong sensitivity of ozone in the plume to chemical composition simulated by the POLMIP  
538 models. We have investigated separately sensitivity to (a) PAN; (b) oVOCs (acetaldehyde, acetone);  
539 and (c) peroxides (H<sub>2</sub>O<sub>2</sub>, CH<sub>3</sub>OOH), using simulations where the initial concentrations of each of  
540 these three sets of species from each POLMIP model are decreased and increased by a factor of 2. A  
541 factor 2 perturbation is consistent with inter-model differences and biases against observations for  
542 these species along the ARCTAS DC8 flight tracks (Emmons et al., 2014). We apply the same  
543 fractional perturbation to each species to directly compare sensitivities of Arctic ozone  
544 photochemistry to uncertainties in their abundances.

545 Ozone sensitivities to initial PAN concentration in the plume demonstrate the potential importance  
546 of model biases in Arctic NO<sub>y</sub> for Arctic tropospheric ozone. Figure 14 shows changes in simulated  
547 ozone and NO<sub>x</sub> evolution in the plume produced by simulations with perturbations to initial PAN.  
548 Increasing and decreasing initial PAN abundance in the plume leads to a reduction in NO<sub>x</sub> and an  
549 increase in NO<sub>x</sub> respectively (Fig. 14b). The consequent impacts on ozone change in the plume  
550 largely depend on the absolute NO<sub>x</sub> concentration, and the magnitude of the NO<sub>x</sub> perturbation

551 brought about by the fractional change in initial PAN. In the TOMCAT, LMDZ-INCA and GMI-  
552 initialised plumes, an increase in initial PAN leads to a shift from slight net ozone loss to net ozone  
553 production of between 0.5 and 1 ppbv over 4 days (Fig. 14b). Model plumes that descend over the 4  
554 days have increased NO<sub>x</sub> sensitivity to the PAN perturbation. Such altitude changes promote  
555 reduced PAN stability and release of NO<sub>2</sub>. This illustrates the potential sensitivity of in-situ Arctic  
556 ozone production in the simulated fire plume to model NO<sub>y</sub> partitioning errors. Increasing and  
557 decreasing initial oVOC abundances leads to enhancement and suppression of ozone loss in the  
558 plume respectively over the following 4 days (Fig. 14c and d), due to the role of acetaldehyde and  
559 acetone as a source of the peroxyacetyl radical during their photo-oxidation. This promotes the  
560 formation of PAN, reducing NO<sub>x</sub> concentrations in the plume. Consequently, model plumes in which  
561 NO<sub>x</sub> concentrations are large enough to promote ozone production show larger ozone sensitivity to  
562 this perturbation. These results suggest that after having undergone export from the continental  
563 boundary layer and long-range transport into the Arctic, PAN formation and loss may still play an  
564 important role in ozone photochemistry in such plumes. In plumes with very low NO<sub>x</sub> abundances,  
565 and dominated by ozone loss, perturbation to initial peroxide concentrations produces a larger  
566 effect on ozone (approx. ±0.5 ppbv over 4 days in the CAM5-chem plume) (Fig. 14e). Increased and  
567 decreased peroxide leads to increases and decreases in HO<sub>2</sub> production from peroxide photolysis,  
568 resulting in changes to the rate of ozone loss via O<sub>3</sub> + HO<sub>2</sub>. Increased initial peroxide concentrations  
569 also lead to enhanced removal of NO<sub>x</sub> in the plume, due to increased HO<sub>x</sub> production (Fig. 14f).

570

571

## 572 **5. Summary and conclusions**

573 We have evaluated tropospheric ozone enhancement in air dominated by biomass burning  
574 emissions at high latitudes (> 50N) in the summer, using simulations from the POLMIP multi-model  
575 comparison exercise for July 2008. Using 25-day fixed lifetime CO tracers emitted from fires and  
576 anthropogenic sources in the models, we calculated  $\Delta O_3/\Delta CO$  enhancement ratios in air dominated  
577 by fire emissions. All POLMIP models that simulated fixed-lifetime tracers demonstrate positive  
578 ozone enhancement in fire-dominated air, with ozone enhancement increasing with air mass age on  
579 average in the models, suggesting net tropospheric ozone production in biomass burning air masses  
580 transported to the Arctic.  $\Delta O_3/\Delta CO$  values ranged between 0.039 and 0.196 ppbv/ppbv (mean: 0.113  
581 ppbv/ppbv) in the younger air, and between 0.140 and 0.261 ppbv/ppbv (mean: 0.193 ppbv) in the  
582 more aged air, with age since emission defined by the ratio of propane to ethane mixing ratios.  
583 These values are in broad agreement with the range of observational estimates from the literature,

584 and larger than those in some previous modelling studies. Model NO<sub>y</sub> partitioning may play an  
585 important role in determining lower model-diagnosed ozone production efficiencies.

586 Model  $\Delta$ PAN/ $\Delta$ CO enhancement ratios at high latitudes show distinct groupings according to the  
587 meteorological data used to drive the models. ECMWF-forced models produce larger  $\Delta$ PAN/ $\Delta$ CO  
588 values (4.44-6.28 pptv/ppbv) than GEOS5-forced models (2.02-3.02 pptv/ppbv), which we show is  
589 likely linked to differences in the efficiency of vertical transport during poleward export from mid-  
590 latitude source regions. Comparison with limited observations from the ARCTAS-B aircraft campaign  
591 suggests that the larger PAN enhancement ratios simulated by the ECMWF-forced models are  
592 consistent with the majority of these observations. We find little relationship between the efficiency  
593 of Arctic PAN import in fire-dominated air and Arctic ozone enhancement across the diverse range of  
594 POLMIP models. However, among three models using the same chemistry scheme there is a general  
595 increase in  $\Delta$ O<sub>3</sub>/ $\Delta$ CO with increased PAN import efficiency.

596 All POLMIP models are capable of resolving a large plume of mixed Asian anthropogenic and Siberian  
597 fire pollution, which is imported to the Arctic on July 7<sup>th</sup> 2008, with close similarities in simulated  
598 horizontal structure. These features are in good agreement with CO observations from the IASI  
599 satellite instrument and the FLEXPART Lagrangian particle dispersion model, shown in a previous  
600 study (Sodemann et al., 2011). Fixed-lifetime tracers simulated by the models show that the leading  
601 edge of this plume is dominated by fire emissions in all POLMIP models. Simulations using a  
602 Lagrangian chemical transport model show that 4-day net ozone change in the plume is sensitive to  
603 differences in plume chemical composition and plume vertical position among the POLMIP models.  
604 In particular, Arctic ozone evolution in the plume is highly sensitive to initial concentrations of PAN,  
605 as well as oxygenated VOCs (acetone, acetaldehyde), due to their role in producing the peroxyacetyl  
606 radical PAN precursor. Vertical displacement is also important due to its effects on the stability of  
607 PAN, and subsequent effect on NO<sub>x</sub> abundance. In plumes where net ozone production is limited,  
608 we find that the lifetime of ozone in the plume is sensitive to hydrogen peroxide loading, due to the  
609 production of HO<sub>2</sub> from peroxide photolysis, and the key role of HO<sub>2</sub> + O<sub>3</sub> in controlling ozone loss.

610 Overall, our results suggest that emissions from biomass burning lead to large-scale enhancement in  
611 high latitude NO<sub>y</sub> and tropospheric ozone during summer, with increasing production of ozone as air  
612 masses age, and that this is consistent across a wide range of chemical transport models using the  
613 same emissions data. In addition, model deficiencies and inter-model differences in simulating  
614 species that are less commonly observed in the Arctic (PANs, oxygenated VOCs, and peroxides) are  
615 important to understand due to their substantial roles in governing in-situ ozone production and loss  
616 in plumes imported to the summertime Arctic troposphere.

617 **Acknowledgements**

618 SRA acknowledges support from the NCAR Advanced Study Program via a Faculty Fellowship award, and the  
619 NCAR Atmospheric Chemistry Division. SRA and SAM were supported by the EurEX project, funded by the UK  
620 Natural Environment Research Council (ref: NE/H020241/1). LKE and S. Tilmes acknowledge the National  
621 Center for Atmospheric Research, which is sponsored by the U.S. National Science Foundation. Author LKE  
622 acknowledges support from the National Aeronautics and Space Administration under Award No.  
623 NNX08AD22G issued through the Science Mission Directorate, Tropospheric Composition Program. Authors  
624 K.S.L., J.L.T., S.Turquety and Y.L. acknowledge support from projects Agence National de Recherche (ANR)  
625 Climate Impact of Short-lived Climate Forcers and Methane in the Arctic (CLIMSLIP) Blanc SIMI 5-6 021 01 and  
626 CLIMSLIP-LEFE (CNRS-INSU). VH acknowledges funding from the European Union's Seventh Framework  
627 Programme (FP7) under Grant Agreement no 283576. Contributions from the Swedish Meteorological and  
628 Hydrological Institute were funded by the Swedish Environmental Protection Agency under contract NV-  
629 09414-12 and through the Swedish Climate and Clean Air research program, SCAC.

630 **References**

631 Alvarado, M. J., Logan, J. A., Mao, J., Apel, E., Riemer, D., Blake, D., Cohen, R. C., Min, K. E., Perring,  
632 A. E., Browne, E. C., Wooldridge, P. J., Diskin, G. S., Sachse, G. W., Fuelberg, H., Sessions, W. R.,  
633 Harrigan, D. L., Huey, G., Liao, J., Case-Hanks, A., Jimenez, J. L., Cubison, M. J., Vay, S. A.,  
634 Weinheimer, A. J., Knapp, D. J., Montzka, D. D., Flocke, F. M., Pollack, I. B., Wennberg, P. O., Kurten,  
635 A., Crouse, J., St Clair, J. M., Wisthaler, A., Mikoviny, T., Yantosca, R. M., Carouge, C. C., and Le  
636 Sager, P.: Nitrogen oxides and PAN in plumes from boreal fires during ARCTAS-B and their impact on  
637 ozone: an integrated analysis of aircraft and satellite observations, *Atmospheric Chemistry and  
638 Physics*, 10, 9739-9760, 2010.

639 Andreae, M. O., Browell, E. V., Garstang, M., Gregory, G. L., Harriss, R. C., Hill, G. F., Jacob, D. J.,  
640 Pereira, M. C., Sachse, G. W., Setzer, A. W., Dias, P. L. S., Talbot, R. W., Torres, A. L., and Wofsy, S. C.:  
641 Biomass-burning emissions and associated haze layers over Amazonia, *Journal of Geophysical  
642 Research: Atmospheres*, 93, 1509-1527, 1988.

643 Atkinson, R., Baulch, D. L., Cox, R. A., Crowley, J. N., Hampson, R. F., Hynes, R. G., Jenkin, M. E., Rossi,  
644 M. J., Troe, J., and Subcommittee, I.: Evaluated kinetic and photochemical data for atmospheric  
645 chemistry: Volume II &ndash; gas phase reactions of organic species, *Atmos. Chem. Phys.*, 6, 3625-  
646 4055, 2006.

647 Bertschi, I. T., Jaffe, D. A., Jaegle, L., Price, H. U., and Dennison, J. B.: PHOBEA/ITCT 2002 airborne  
648 observations of transpacific transport of ozone, CO, volatile organic compounds, and aerosols to the  
649 northeast Pacific: Impacts of Asian anthropogenic and Siberian boreal fire emissions, *Journal of  
650 Geophysical Research-Atmospheres*, 109, 2004.

651 Bourgeois, Q. and Bey, I.: Pollution transport efficiency toward the Arctic: Sensitivity to aerosol  
652 scavenging and source regions, *Journal of Geophysical Research-Atmospheres*, 116, 2011.

653 Calvert, J. G.: HYDROCARBON INVOLVEMENT IN PHOTOCHEMICAL SMOG FORMATION IN LOS-  
654 ANGELES ATMOSPHERE, *Environ. Sci. Technol.*, 10, 256-262, 1976.

655 de Groot, W. J., Flannigan, M. D., and Cantin, A. S.: Climate change impacts on future boreal fire  
656 regimes, *For. Ecol. Manage.*, 294, 35-44, 2013.

657 Fischer, E. V., Jacob, D. J., Yantosca, R. M., Sulprizio, M. P., Millet, D. B., Mao, J., Paulot, F., Singh, H.  
658 B., Roiger, A., Ries, L., Talbot, R. W., Dzepina, K., and Pandey Deolal, S.: Atmospheric peroxyacetyl  
659 nitrate (PAN): a global budget and source attribution, *Atmos. Chem. Phys.*, 14, 2679-2698, 2014.

660 Fisher, J. A., Jacob, D. J., Purdy, M. T., Kopacz, M., Le Sager, P., Carouge, C., Holmes, C. D., Yantosca,  
661 R. M., Batchelor, R. L., Strong, K., Diskin, G. S., Fuelberg, H. E., Holloway, J. S., Hyer, E. J., McMillan,  
662 W. W., Warner, J., Streets, D. G., Zhang, Q., Wang, Y., and Wu, S.: Source attribution and interannual  
663 variability of Arctic pollution in spring constrained by aircraft (ARCTAS, ARCPAC) and satellite (AIRS)  
664 observations of carbon monoxide, *Atmos. Chem. Phys.*, 10, 977-996, 2010.

665 Goode, J. G., Yokelson, R. J., Ward, D. E., Susott, R. A., Babbitt, R. E., Davies, M. A., and Hao, W. M.:  
666 Measurements of excess O<sub>3</sub>, CO<sub>2</sub>, CO, CH<sub>4</sub>, C<sub>2</sub>H<sub>4</sub>, C<sub>2</sub>H<sub>2</sub>, HCN, NO, NH<sub>3</sub>, HCOOH, CH<sub>3</sub>COOH, HCHO,  
667 and CH<sub>3</sub>OH in 1997 Alaskan biomass burning plumes by airborne fourier transform infrared  
668 spectroscopy (AFTIR), *Journal of Geophysical Research-Atmospheres*, 105, 22147-22166, 2000.

669 Honrath, R. E., Owen, R. C., Val Martin, M., Reid, J. S., Lapina, K., Fialho, P., Dziobak, M. P., Kleissl, J.,  
670 and Westphal, D. L.: Regional and hemispheric impacts of anthropogenic and biomass burning  
671 emissions on summertime CO and O<sub>3</sub> in the North Atlantic lower free troposphere, *Journal of*  
672 *Geophysical Research-Atmospheres*, 109, 2004.

673 Hornbrook, R. S., Blake, D. R., Diskin, G. S., Fried, A., Fuelberg, H. E., Meinardi, S., Mikoviny, T.,  
674 Richter, D., Sachse, G. W., Vay, S. A., Walega, J., Weibring, P., Weinheimer, A. J., Wiedinmyer, C.,  
675 Wisthaler, A., Hills, A., Riemer, D. D., and Apel, E. C.: Observations of nonmethane organic  
676 compounds during ARCTAS - Part 1: Biomass burning emissions and plume enhancements,  
677 *Atmospheric Chemistry and Physics*, 11, 11103-11130, 2011.

678 Jacob, D. J., Crawford, J. H., Maring, H., Clarke, A. D., Dibb, J. E., Emmons, L. K., Ferrare, R. A.,  
679 Hostetler, C. A., Russell, P. B., Singh, H. B., Thompson, A. M., Shaw, G. E., McCauley, E., Pederson, J.  
680 R., and Fisher, J. A.: The Arctic Research of the Composition of the Troposphere from Aircraft and  
681 Satellites (ARCTAS) mission: design, execution, and first results, *Atmospheric Chemistry and Physics*,  
682 10, 5191-5212, 2010.

683 Jacob, D. J., Wofsy, S. C., Bakwin, P. S., Fan, S. M., Harriss, R. C., Talbot, R. W., Bradshaw, J. D.,  
684 Sandholm, S. T., Singh, H. B., Browell, E. V., Gregory, G. L., Sachse, G. W., Shipham, M. C., Blake, D. R.,  
685 and Fitzjarrald, D. R.: Summertime photochemistry of the troposphere at high northern latitudes,  
686 *Journal of Geophysical Research: Atmospheres*, 97, 16421-16431, 1992.

687 Jaffe, D. A. and Wigder, N. L.: Ozone production from wildfires: A critical review, *Atmospheric*  
688 *Environment*, 51, 1-10, 2012.

689 Lamarque, J. F., Bond, T. C., Eyring, V., Granier, C., Heil, A., Klimont, Z., Lee, D., Liousse, C., Mieville,  
690 A., Owen, B., Schultz, M. G., Shindell, D., Smith, S. J., Stehfest, E., Van Aardenne, J., Cooper, O. R.,  
691 Kainuma, M., Mahowald, N., McConnell, J. R., Naik, V., Riahi, K., and van Vuuren, D. P.: Historical  
692 (1850–2000) gridded anthropogenic and biomass burning emissions of reactive gases and aerosols:  
693 methodology and application, *Atmos. Chem. Phys.*, 10, 7017-7039, 2010.

694 Liang, Q., Rodriguez, J. M., Douglass, A. R., Crawford, J. H., Olson, J. R., Apel, E., Bian, H., Blake, D. R.,  
695 Brune, W., Chin, M., Colarco, P. R., da Silva, A., Diskin, G. S., Duncan, B. N., Huey, L. G., Knapp, D. J.,  
696 Montzka, D. D., Nielsen, J. E., Pawson, S., Riemer, D. D., Weinheimer, A. J., and Wisthaler, A.:  
697 Reactive nitrogen, ozone and ozone production in the Arctic troposphere and the impact of  
698 stratosphere-troposphere exchange, *Atmospheric Chemistry and Physics*, 11, 13181-13199, 2011.

699 Mao, J. Q., Horowitz, L. W., Naik, V., Fan, S. M., Liu, J. F., and Fiore, A. M.: Sensitivity of tropospheric  
700 oxidants to biomass burning emissions: implications for radiative forcing, *Geophysical Research*  
701 *Letters*, 40, 1241-1246, 2013a.

702 Mao, J., Fan, S., Jacob, D. J., and Travis, K. R.: Radical loss in the atmosphere from Cu- Fe redox  
703 coupling in aerosols, *Atmos. Chem. Phys.*, 13, 509–519, doi:10.5194/acp-13- 509-2013, 2013b.

704 Martin, M. V., Honrath, R. E., Owen, R. C., Pfister, G., Fialho, P., and Barata, F.: Significant  
705 enhancements of nitrogen oxides, black carbon, and ozone in the North Atlantic lower free  
706 troposphere resulting from North American boreal wildfires, *Journal of Geophysical Research-*  
707 *Atmospheres*, 111, 2006.

708 Mauzerall, D. L., Jacob, D. J., Fan, S. M., Bradshaw, J. D., Gregory, G. L., Sachse, G. W., and Blake, D.  
709 R.: Origin of tropospheric ozone at remote high northern latitudes in summer, *Journal of Geophysical*  
710 *Research-Atmospheres*, 101, 4175-4188, 1996.

711 Methven, J., Arnold, S. R., O'Connor, F. M., Barjat, H., Dewey, K., Kent, J., and Brough, N.: Estimating  
712 photochemically produced ozone throughout a domain using flight data and a Lagrangian model,  
713 *Journal of Geophysical Research-Atmospheres*, 108, 2003.

714 Monks, S. A., Arnold, S. R., and Chipperfield, M. P.: Evidence for El Nino-Southern Oscillation (ENSO)  
715 influence on Arctic CO interannual variability through biomass burning emissions, *Geophysical*  
716 *Research Letters*, 39, 2012.

717 Naik, V., Voulgarakis, A., Fiore, A. M., Horowitz, L. W., Lamarque, J.-F., Lin, M., Prather, M. J., Young,  
718 P. J., Bergmann, D., Cameron-Smith, P. J., Cionni, I., Collins, W. J., Dalsøren, S. B., Doherty, R., Eyring,  
719 V., Faluvegi, G., Folberth, G. A., Josse, B., Lee, Y. H., MacKenzie, I. A., Nagashima, T., van Noije, T. P.  
720 C., Plummer, D. A., Righi, M., Rumbold, S. T., Skeie, R., Shindell, D. T., Stevenson, D. S., Strode, S.,  
721 Sudo, K., Szopa, S., and Zeng, G.: Preindustrial to present-day changes in tropospheric hydroxyl  
722 radical and methane lifetime from the Atmospheric Chemistry and Climate Model  
723 Intercomparison Project (ACCMIP), *Atmos. Chem. Phys.*, 13, 5277-5298, doi:10.5194/acp-13-5277-  
724 2013, 2013.

725 Olson, J. R., Crawford, J. H., Brune, W., Mao, J., Ren, X., Fried, A., Anderson, B., Apel, E., Beaver, M.,  
726 Blake, D., Chen, G., Crouse, J., Dibb, J., Diskin, G., Hall, S. R., Huey, L. G., Knapp, D., Richter, D.,  
727 Riemer, D., Clair, J. S., Ullmann, K., Walega, J., Weibring, P., Weinheimer, A., Wennberg, P., and  
728 Wisthaler, A.: An analysis of fast photochemistry over high northern latitudes during spring and  
729 summer using in-situ observations from ARCTAS and TOPSE, *Atmospheric Chemistry and Physics*, 12,  
730 6799-6825, 2012.

731 Paris, J. D., Stohl, A., Nedelec, P., Arshinov, M. Y., Panchenko, M. V., Shmargunov, V. P., Law, K. S.,  
732 Belan, B. D., and Ciais, P.: Wildfire smoke in the Siberian Arctic in summer: source characterization  
733 and plume evolution from airborne measurements, *Atmospheric Chemistry and Physics*, 9, 9315-  
734 9327, 2009.

735 Parrella, J. P., Jacob, D. J., Liang, Q., Zhang, Y., Mickley, L. J., Miller, B., Evans, M. J., Yang, X., Pyle, J.  
736 A., Theys, N., and Van Roozendael, M.: Tropospheric bromine chemistry: implications for present  
737 and pre-industrial ozone and mercury, *Atmos. Chem. Phys.*, 12, 6723-6740, 2012.

738 Parrington, M., Palmer, P. I., Henze, D. K., Tarasick, D. W., Hyer, E. J., Owen, R. C., Helmig, D.,  
739 Clerbaux, C., Bowman, K. W., Deeter, M. N., Barratt, E. M., Coheur, P. F., Hurtmans, D., Jiang, Z.,  
740 George, M., and Worden, J. R.: The influence of boreal biomass burning emissions on the distribution  
741 of tropospheric ozone over North America and the North Atlantic during 2010, *Atmospheric*  
742 *Chemistry and Physics*, 12, 2077-2098, 2012.

743 Parrington, M., Palmer, P. I., Lewis, A. C., Lee, J. D., Rickard, A. R., Di Carlo, P., Taylor, J. W., Hopkins,  
744 J. R., Punjabi, S., Oram, D. E., Forster, G., Aruffo, E., Moller, S. J., Bauguitte, S. J. B., Allan, J. D., Coe,  
745 H., and Leigh, R. J.: Ozone photochemistry in boreal biomass burning plumes, *Atmospheric*  
746 *Chemistry and Physics*, 13, 7321-7341, 2013.

747 Pfister, G. G., Emmons, L. K., Hess, P. G., Honrath, R., Lamarque, J. F., Martin, M. V., Owen, R. C.,  
748 Avery, M. A., Browell, E. V., Holloway, J. S., Nedelec, P., Purvis, R., Ryerson, T. B., Sachse, G. W., and  
749 Schlager, H.: Ozone production from the 2004 North American boreal fires, *Journal of Geophysical*  
750 *Research-Atmospheres*, 111, 2006.

751 Pommier, M., Law, K. S., Clerbaux, C., Turquety, S., Hurtmans, D., Hadji-Lazaro, J., Coheur, P. F.,  
752 Schlager, H., Ancellet, G., Paris, J. D., Nédélec, P., Diskin, G. S., Podolske, J. R., Holloway, J. S., and  
753 Bernath, P.: IASI carbon monoxide validation over the Arctic during POLARCAT spring and summer  
754 campaigns, *Atmos. Chem. Phys.*, 10, 10655-10678, 2010.

755 Pugh, T. A. M., Cain, M., Methven, J., Wild, O., Arnold, S. R., Real, E., Law, K. S., Emmerson, K. M.,  
756 Owen, S. M., Pyle, J. A., Hewitt, C. N., and MacKenzie, A. R.: A Lagrangian model of air-mass  
757 photochemistry and mixing using a trajectory ensemble: the Cambridge Tropospheric Trajectory  
758 model of Chemistry And Transport (CiTTyCAT) version 4.2, *Geoscientific Model Development*, 5, 193-  
759 221, 2012.

760 Quinn, P. K., Bates, T. S., Baum, E., Doubleday, N., Fiore, A. M., Flanner, M., Fridlind, A., Garrett, T. J.,  
761 Koch, D., Menon, S., Shindell, D., Stohl, A., and Warren, S. G.: Short-lived pollutants in the Arctic:

762 their climate impact and possible mitigation strategies, *Atmospheric Chemistry and Physics*, 8, 1723-  
763 1735, 2008.

764 Real, E., Law, K. S., Weinzierl, B., Fiebig, M., Petzold, A., Wild, O., Methven, J., Arnold, S., Stohl, A.,  
765 Huntrieser, H., Roiger, A., Schlager, H., Stewart, D., Avery, M., Sachse, G., Browell, E., Ferrare, R., and  
766 Blake, D.: Processes influencing ozone levels in Alaskan forest fire plumes during long-range  
767 transport over the North Atlantic, *Journal of Geophysical Research-Atmospheres*, 112, 2007.

768 Roiger, A., Schlager, H., Schafner, A., Huntrieser, H., Scheibe, M., Aufmhoff, H., Cooper, O. R.,  
769 Sodemann, H., Stohl, A., Burkhardt, J., Lazzara, M., Schiller, C., Law, K. S., and Arnold, F.: In-situ  
770 observation of Asian pollution transported into the Arctic lowermost stratosphere, *Atmospheric  
771 Chemistry and Physics*, 11, 10975-10994, 2011.

772 Shindell, D.: Local and remote contributions to Arctic warming, *Geophysical Research Letters*, 34,  
773 2007.

774 Shindell, D. and Faluvegi, G.: Climate response to regional radiative forcing during the twentieth  
775 century, *Nat. Geosci.*, 2, 294-300, 2009.

776 Shindell, D. T., Chin, M., Dentener, F., Doherty, R. M., Faluvegi, G., Fiore, A. M., Hess, P., Koch, D. M.,  
777 MacKenzie, I. A., Sanderson, M. G., Schultz, M. G., Schulz, M., Stevenson, D. S., Teich, H., Textor, C.,  
778 Wild, O., Bergmann, D. J., Bey, I., Bian, H., Cuvelier, C., Duncan, B. N., Folberth, G., Horowitz, L. W.,  
779 Jonson, J., Kaminski, J. W., Marmor, E., Park, R., Pringle, K. J., Schroeder, S., Szopa, S., Takemura, T.,  
780 Zeng, G., Keating, T. J., and Zuber, A.: A multi-model assessment of pollution transport to the Arctic,  
781 *Atmospheric Chemistry and Physics*, 8, 5353-5372, 2008.

782 Singh, H. B., Anderson, B. E., Brune, W. H., Cai, C., Cohen, R. C., Crawford, J. H., Cubison, M. J., Czech,  
783 E. P., Emmons, L., Fuelberg, H. E., Huey, G., Jacob, D. J., Jimenez, J. L., Kaduwela, A., Kondo, Y., Mao,  
784 J., Olson, J. R., Sachse, G. W., Vay, S. A., Weinheimer, A., Wennberg, P. O., Wisthaler, A., and Team,  
785 A. S.: Pollution influences on atmospheric composition and chemistry at high northern latitudes:  
786 Boreal and California forest fire emissions, *Atmospheric Environment*, 44, 4553-4564, 2010.

787 Singh, H. B. and Hanst, P. L.: PEROXYACETYL NITRATE (PAN) IN THE UNPOLLUTED ATMOSPHERE - AN  
788 IMPORTANT RESERVOIR FOR NITROGEN-OXIDES, *Geophysical Research Letters*, 8, 941-944, 1981.

789 Singh, H. B., O'Hara, D., Herlth, D., Bradshaw, J. D., Sandholm, S. T., Gregory, G. L., Sachse, G. W.,  
790 Blake, D. R., Crutzen, P. J., and Kanakidou, M. A.: Atmospheric measurements of peroxyacetyl nitrate  
791 and other organic nitrates at high latitudes: Possible sources and sinks, *Journal of Geophysical  
792 Research: Atmospheres*, 97, 16511-16522, 1992.

793 Sodemann, H., Pommier, M., Arnold, S. R., Monks, S. A., Stebel, K., Burkhardt, J. F., Hair, J. W., Diskin,  
794 G. S., Clerbaux, C., Coheur, P. F., Hurtmans, D., Schlager, H., Blechschmidt, A. M., Kristjansson, J. E.,  
795 and Stohl, A.: Episodes of cross-polar transport in the Arctic troposphere during July 2008 as seen  
796 from models, satellite, and aircraft observations, *Atmospheric Chemistry and Physics*, 11, 3631-3651,  
797 2011.

798 Tanimoto, H., Matsumoto, K., and Uematsu, M.: Ozone-CO Correlations in Siberian Wildfire Plumes  
799 Observed at Rishiri Island, *Sola*, 4, 65-68, 2008.

800 Thomas, J. L., Raut, J. C., Law, K. S., Marelle, L., Ancellet, G., Ravetta, F., Fast, J. D., Pfister, G.,  
801 Emmons, L. K., Diskin, G. S., Weinheimer, A., Roiger, A., and Schlager, H.: Pollution transport from  
802 North America to Greenland during summer 2008, *Atmospheric Chemistry and Physics*, 13, 3825-  
803 3848, 2013.

804 van der Werf, G. R., Randerson, J. T., Giglio, L., Collatz, G. J., Mu, M., Kasibhatla, P. S., Morton, D. C.,  
805 DeFries, R. S., Jin, Y., and van Leeuwen, T. T.: Global fire emissions and the contribution of  
806 deforestation, savanna, forest, agricultural, and peat fires (1997-2009), *Atmospheric Chemistry and  
807 Physics*, 10, 11707-11735, 2010.

808 Voulgarakis, A., Telford, P. J., Aghedo, A. M., Braesicke, P., Faluvegi, G., Abraham, N. L., Bowman, K.  
809 W., Pyle, J. A., and Shindell, D. T.: Global multi-year O<sub>3</sub>-CO correlation patterns from models and TES  
810 satellite observations, *Atmos. Chem. Phys.*, 11, 5819-5838, doi:10.5194/acp-11-5819-2011, 2011.

811 Walker, T. W., Jones, D. B. A., Parrington, M., Henze, D. K., Murray, L. T., Bottenheim, J. W., Anlauf,  
812 K., Worden, J. R., Bowman, K. W., Shim, C., Singh, K., Kopacz, M., Tarasick, D. W., Davies, J., von der

813 Gathen, P., Thompson, A. M., and Carouge, C. C.: Impacts of midlatitude precursor emissions and  
814 local photochemistry on ozone abundances in the Arctic, *Journal of Geophysical Research-*  
815 *Atmospheres*, 117, 2012.

816 Warneke, C., Froyd, K. D., Brioude, J., Bahreini, R., Brock, C. A., Cozic, J., de Gouw, J. A., Fahey, D. W.,  
817 Ferrare, R., Holloway, J. S., Middlebrook, A. M., Miller, L., Montzka, S., Schwarz, J. P., Sodemann, H.,  
818 Spackman, J. R., and Stohl, A.: An important contribution to springtime Arctic aerosol from biomass  
819 burning in Russia, *Geophysical Research Letters*, 37, 2010.

820 Wespes, C., Emmons, L., Edwards, D. P., Hannigan, J., Hurtmans, D., Saunio, M., Coheur, P. F.,  
821 Clerbaux, C., Coffey, M. T., Batchelor, R. L., Lindenmaier, R., Strong, K., Weinheimer, A. J., Nowak, J.  
822 B., Ryerson, T. B., Crouse, J. D., and Wennberg, P. O.: Analysis of ozone and nitric acid in spring and  
823 summer Arctic pollution using aircraft, ground-based, satellite observations and MOZART-4 model:  
824 source attribution and partitioning, *Atmos. Chem. Phys.*, 12, 237-259, 2012.

825 Wofsy, S. C., Sachse, G. W., Gregory, G. L., Blake, D. R., Bradshaw, J. D., Sandholm, S. T., Singh, H. B.,  
826 Barrick, J. A., Harriss, R. C., Talbot, R. W., Shipham, M. A., Browell, E. V., Jacob, D. J., and Logan, J. A.:  
827 ATMOSPHERIC CHEMISTRY IN THE ARCTIC AND SUB-ARCTIC - INFLUENCE OF NATURAL FIRES,  
828 INDUSTRIAL EMISSIONS, AND STRATOSPHERIC INPUTS, *Journal of Geophysical Research-*  
829 *Atmospheres*, 97, 16731-16746, 1992.

830 Zhang, B., Owen, R. C., Perlinger, J. A., Kumar, A., Wu, S., Val Martin, M., Kramer, L., Helmig, D., and  
831 Honrath, R. E.: A semi-Lagrangian view of ozone production tendency in North American outflow in  
832 the summers of 2009 and 2010, *Atmos. Chem. Phys.*, 14, 2267-2287, doi:10.5194/acp-14-2267-2014,  
833 2014.

834

835

836

837 **List of Tables**

838

<b>Model</b>	<b>Resolution</b>	<b>Meteorology</b>	<b>Chemistry</b>
CAM4-Chem	1.925 <sup>o</sup> x 2.5 <sup>o</sup> , 56 levels	GEOS-5	MOZART-4, bulk aerosols
CAM5-Chem	1.9 <sup>o</sup> 25 x 2.5 <sup>o</sup> 25, 56 levels	GEOS-5	MOZART-4, modal aerosols
CIFS	1.125 <sup>o</sup> 25 x 1.125 <sup>o</sup> 25, 60 levels	ECMWF	tropospheric, CB05
GEOS-Chem	225 <sup>o</sup> x 2.5 <sup>o</sup> 25, 47 levels	GEOS-5	tropospheric, 100 species
GMI	2 <sup>o</sup> 25 x 2.5 <sup>o</sup> 25, 72 levels	GEOS-5	stratospheric and tropospheric, 154 species, GOCART aerosols
LMDZ-INCA	1.925 <sup>o</sup> x 3.75 <sup>o</sup> 25, 39 levels	ERA-Interim	tropospheric, 85 species, aerosols
MOZART-4	1.9 <sup>o</sup> 25 x 2.5 <sup>o</sup> , 56 levels	GEOS-5	tropospheric, 103 species, bulk aerosols
TM5	2 <sup>o</sup> 25x 325 <sup>o</sup> , 60 levels	ECMWF	tropospheric, CB05
TOMCAT	2.825 <sup>o</sup> x 2.825 <sup>o</sup> , 31 levels	ECMWF	tropospheric, 82 species
SMHI-MATCH	0.75 <sup>o</sup> x 0.75 <sup>o</sup> , 35 levels (hemispheric)	ECMWF	63 tracers, 110 gas-phase reactions Stratosphere: Monthly means from EU-MACC project (MOZART-4)

839

840 **Table 1:** Description of POLMIP models.

841

	CAM4-Chem	CAM5-Chem	GMI	LMDZ-INCA	MOZART-4	TM5	TOMCAT
Longitude	202.5	200.0	182.5	228.8	172.5	169.5	205.3
Latitude	78.6	78.6	72.0	80.5	76.7	83.0	76.7
Pressure [hPa]	433.8	433.5	737.1	442.7	709.6	422.1	418.1
Ozone [ppbv]	57.8	61.7	62.0	64.8	43.7	53.6	75.6
CO [ppbv]	292.0	280.3	332.3	218.8	251.0	215.8	364.1
NO [pptv]	0.850	1.336	8.731	5.743	0.300	4.974	6.281
NO <sub>2</sub> [pptv]	0.663	1.079	32.473	7.612	5.721	2.618	7.815
HONO <sub>2</sub> [pptv]	4.912	0.757	784.2	288.3	0.093	2.580	463.9
PAN [pptv]	182.7	207.3	93.86	407.1	97.41	448.6	1476.
H <sub>2</sub> O <sub>2</sub> [ppbv]	1.115	1.719	3.492	0.000	1.235	0.000	2.120
MeOOH [ppbv]	0.425	0.579	1.034	0.000	0.836	0.476	0.000
C <sub>2</sub> H <sub>6</sub> [ppbv]	2.165	2.067	2.451	1.642	1.779	1.653	2.637
C <sub>3</sub> H <sub>8</sub> [ppbv]	0.128	0.083	0.130	0.078	0.101	0.082	0.110
Acetone [ppbv]	1.456	1.417	0.000	0.746	1.185	0.345	1.445
Acetaldehyde [ppbv]	0.051	0.046	0.069	0.022	0.126	0.015	0.054
OH [ $10^6$ molec cm <sup>-3</sup> ]	0.42	0.65	1.07	0.45	0.05	0.46	0.48

842

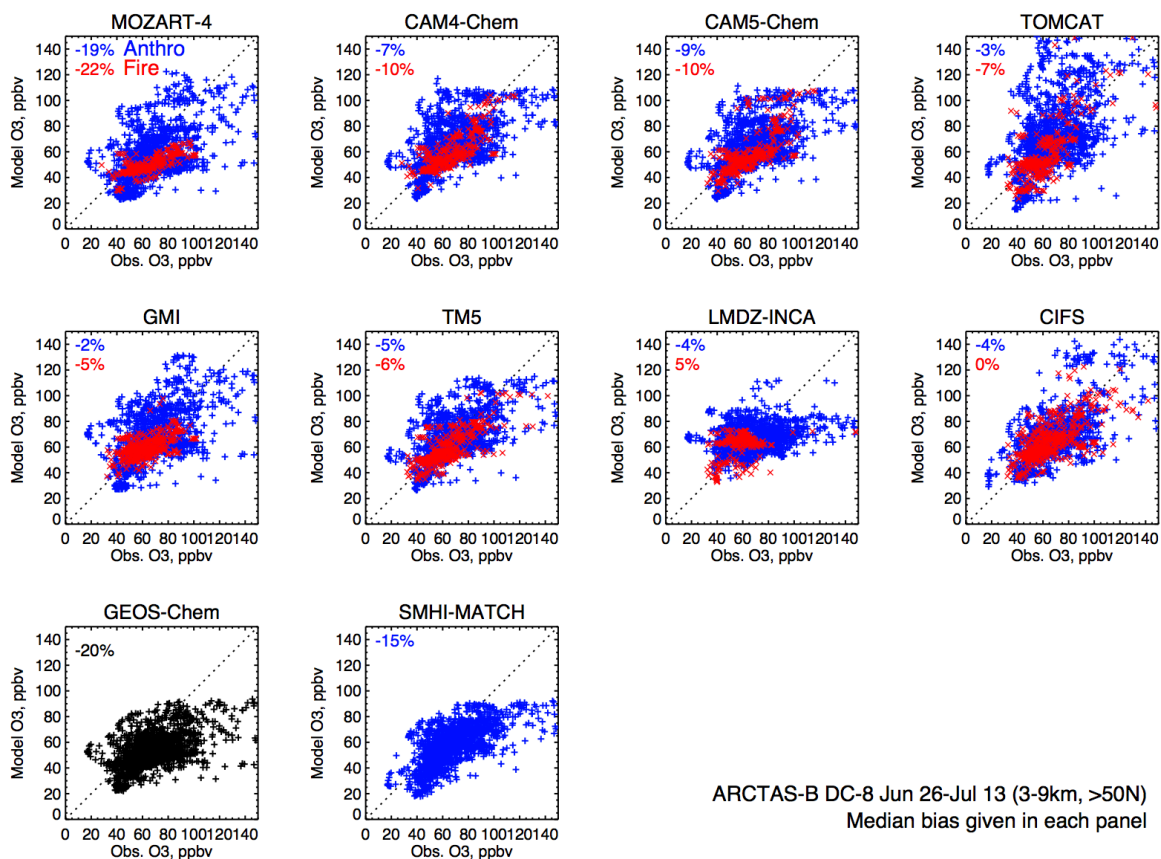
843 **Table 2:** Positions and chemical composition of fire plume maxima in the POLMIP model simulations at 06 UT  
844 on 7<sup>th</sup> July 2008. Plume maxima positions are defined based on abundance of simulated 25-day fixed-lifetime  
845 Asian biomass burning tracer. See text for details.

846

847

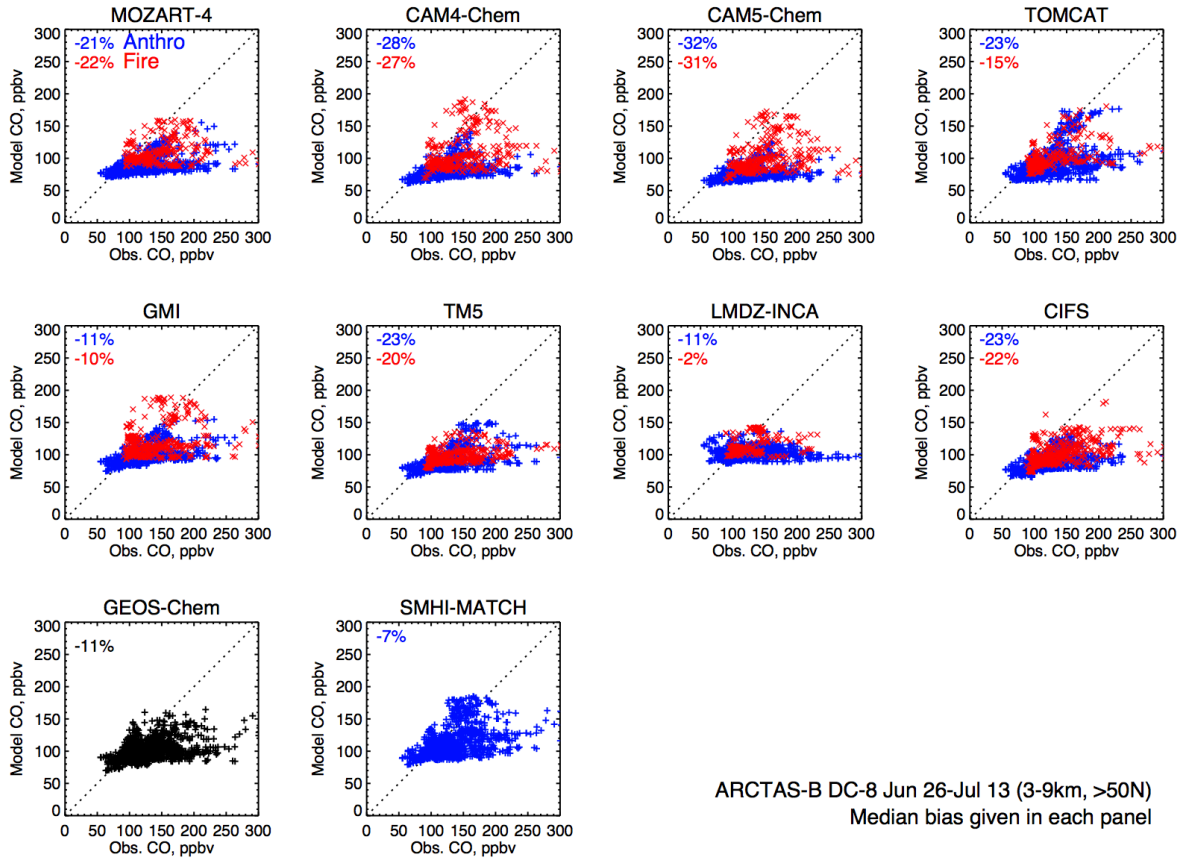
848 **List of Figures**

849



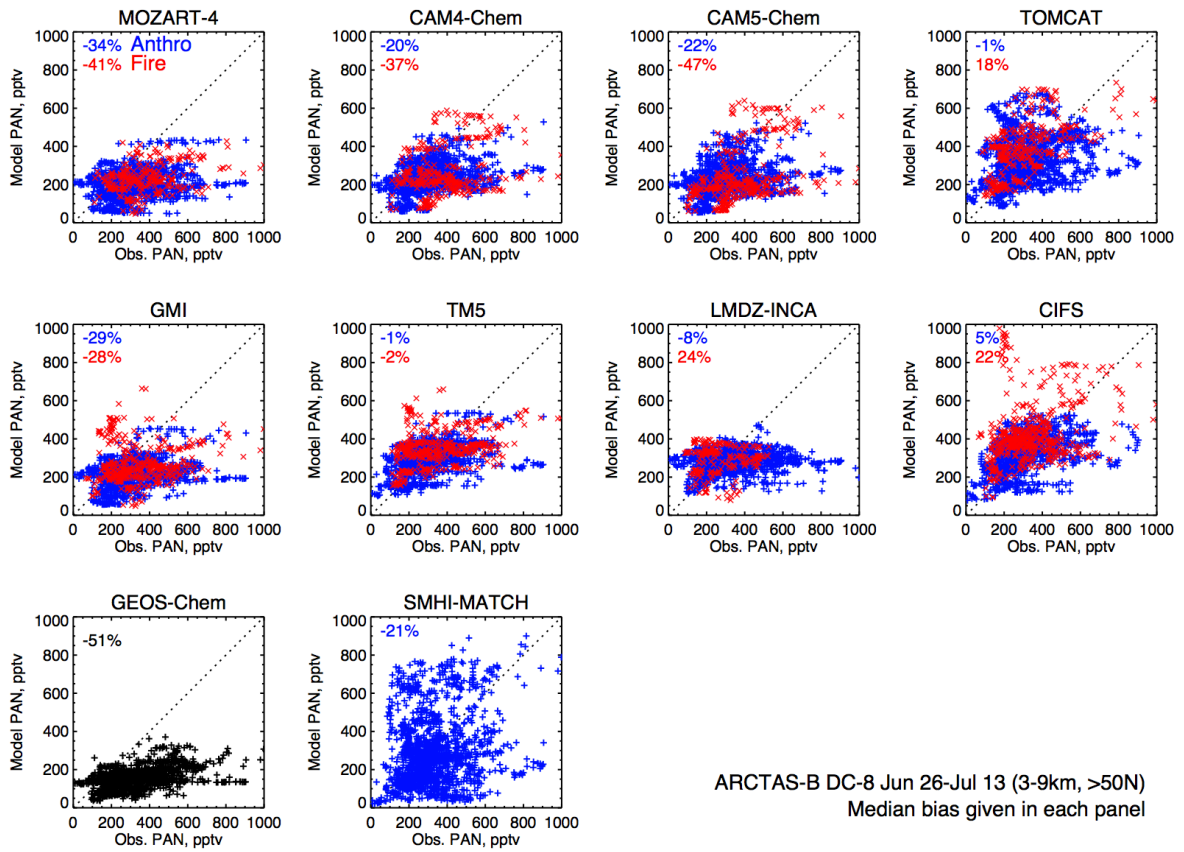
850

851 **Figure 1:** POLMIP model ozone interpolated to selected ARCTAS-B DC8 flight tracks north of 50N,  
 852 and between 3-9km altitude plotted as a function of the DC8-observed concentrations. Blue and red  
 853 colours show model points which are dominated by anthropogenic and biomass burning emissions  
 854 respectively, as diagnosed by 25-day fixed-lifetime CO tracers simulated by the models (see text for  
 855 details). Mean fractional model biases (%) in anthropogenic- and fire-dominated air are shown in  
 856 blue and red text respectively. The GEOS-Chem model did not simulate 25-day fixed lifetime tracers.



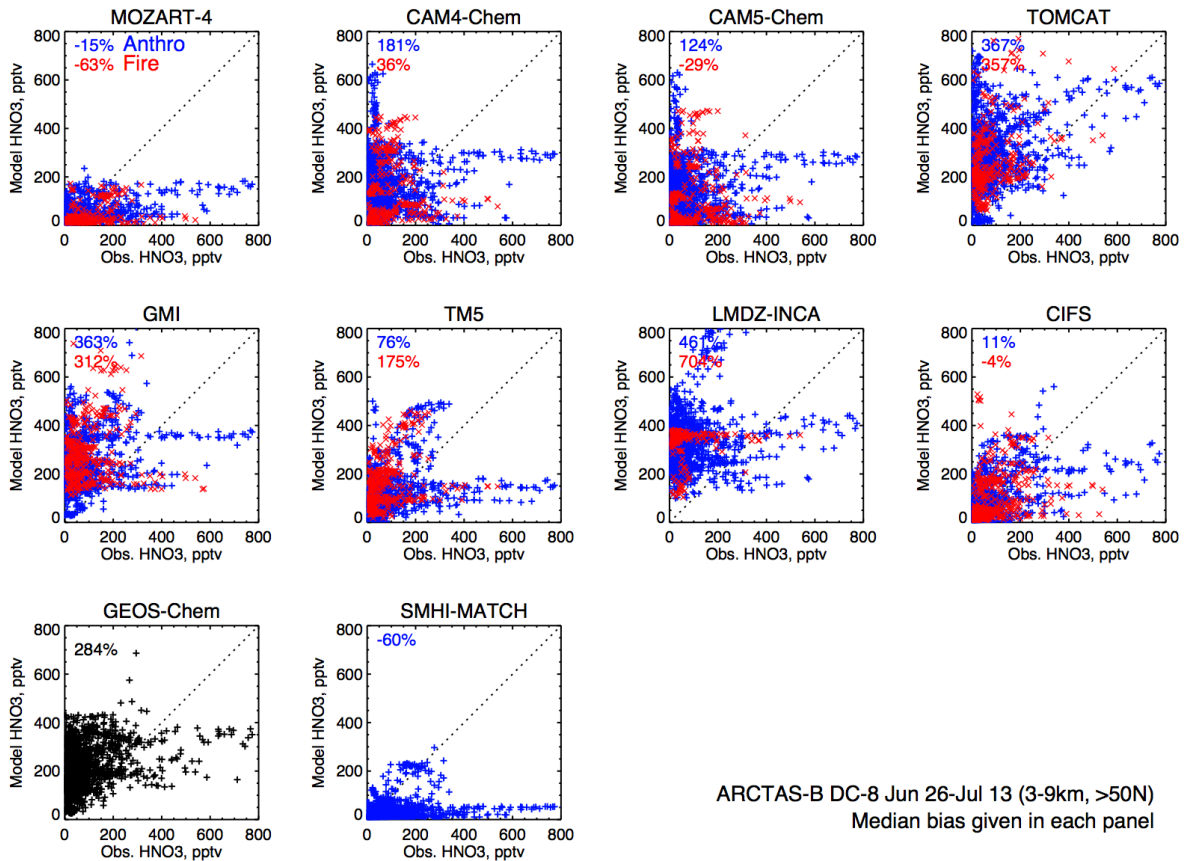
857

858 **Figure 2:** As Fig 1., but for CO.



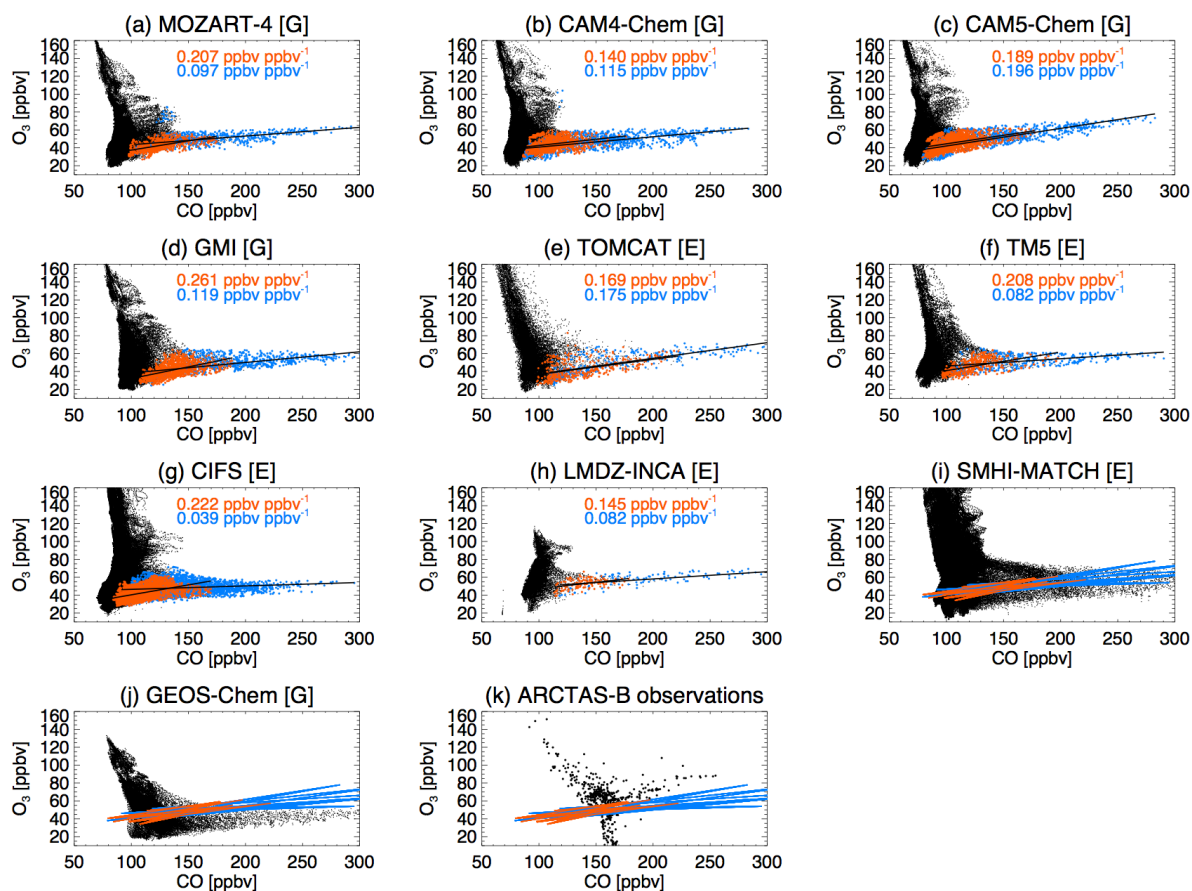
859

860 **Figure 3:** As Fig 1., but for PAN.



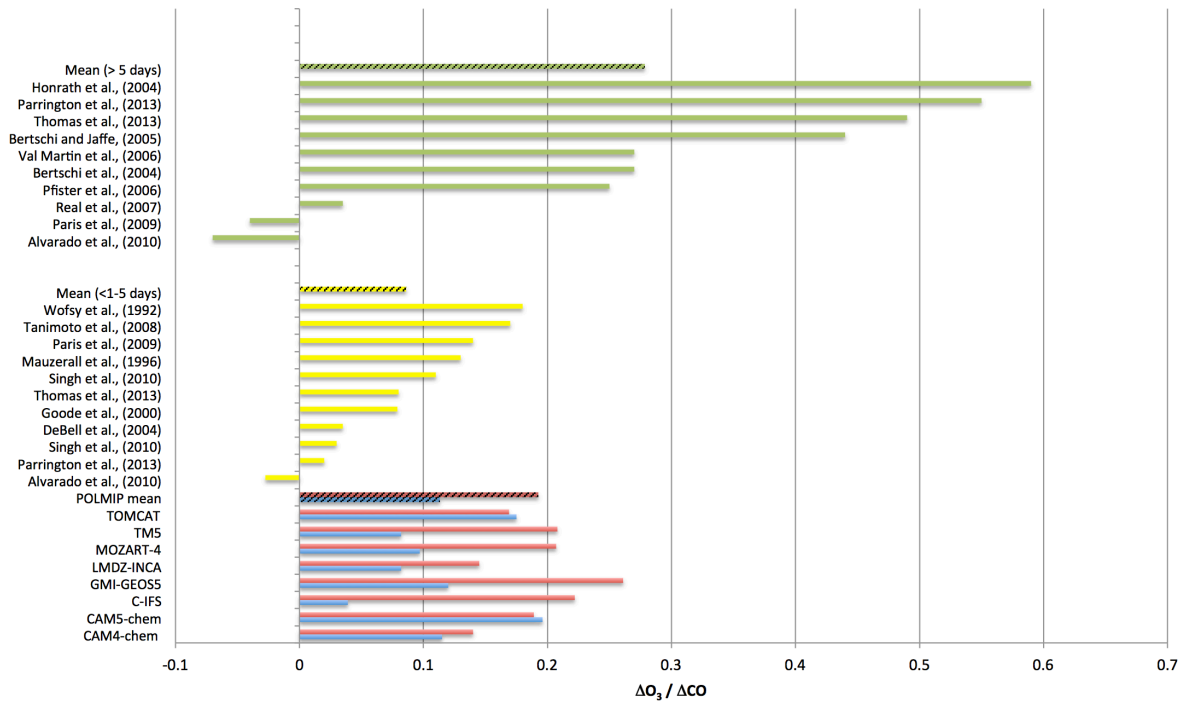
861

862 **Figure 4:** As Fig 1., but for  $\text{HNO}_3$ .



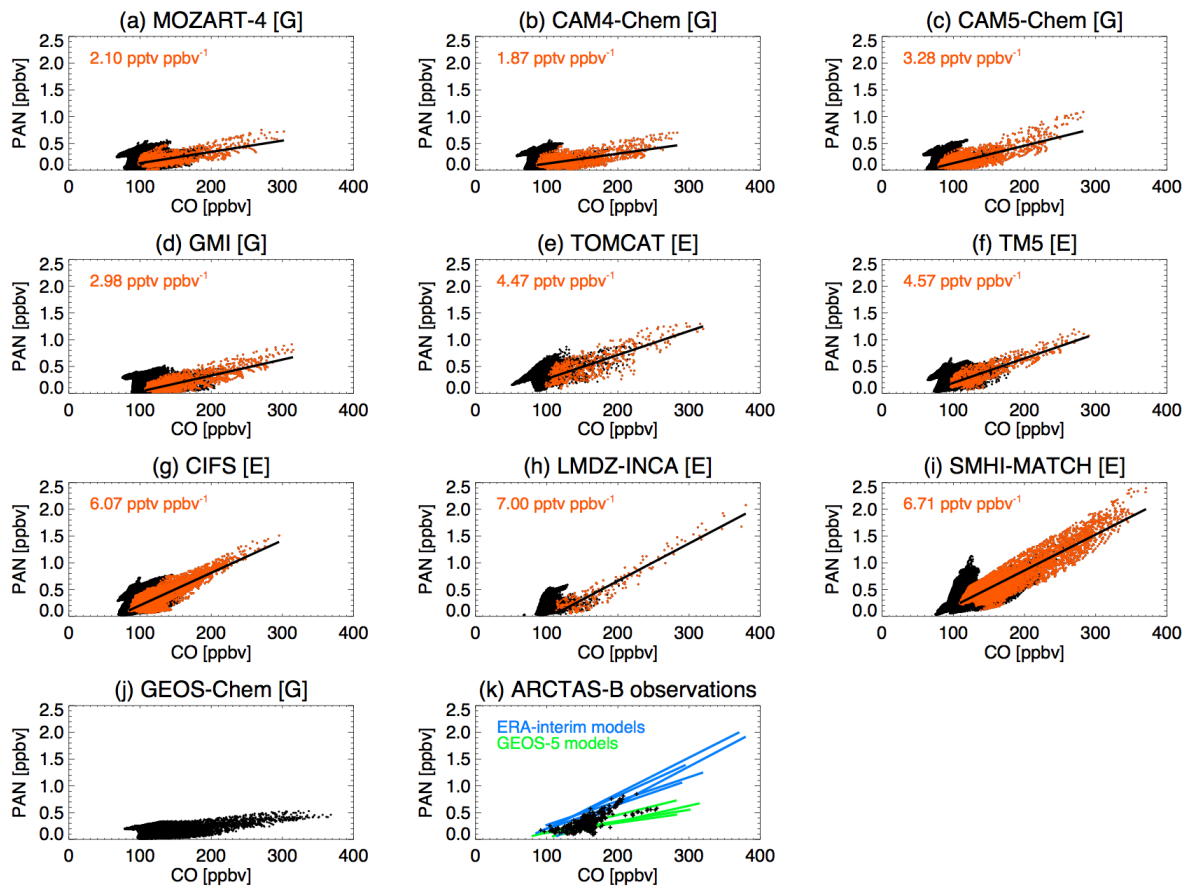
863

864 **Figure 5:** July 2008 monthly-mean  $\text{O}_3$  vs CO from POLMIP model simulations coloured by fire  
865 influence and relative age of air since emission. Black: all points north of 50N, with 850 hPa >  
866 pressure > 250 hPa. Coloured points show model grid boxes where the fire-emitted fixed-lifetime CO  
867 tracer contributes more than 66% of the total (fire + anthropogenic) tracer mixing ratio. Blue and red  
868 points denote younger than average and more aged than average of these points respectively, as  
869 diagnosed by the  $\ln([C3H8]/[C2H6])$  concentration ratio. Models that did not simulate fixed-lifetime  
870 tracers, or do not carry  $[C3H8]$  explicitly, do not have coloured points, but instead show slopes from  
871 linear regressions of the coloured points from the other models (red and blue lines). Red and blue text  
872 give  $\Delta\text{O}_3/\Delta\text{CO}$  slope values from linear regressions of the youngest and most aged populations  
873 respectively. Letters in square brackets denote the meteorological analysis data used to drive the  
874 models - E: ECMWF; G: GEOS-5. Panel (k) shows ARCTAS-B aircraft observations.



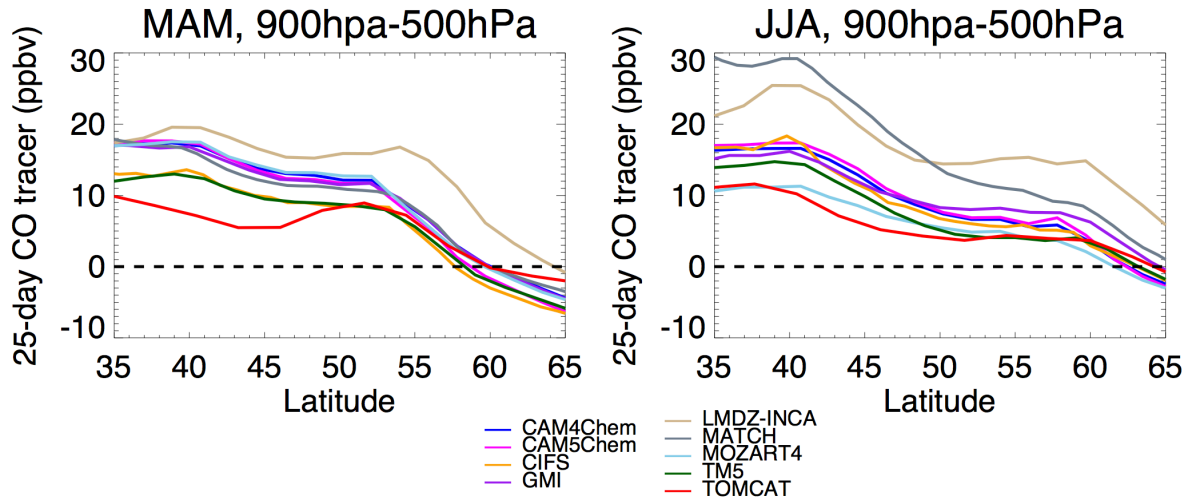
875

876 **Figure 6:**  $\Delta O_3 / \Delta CO$  ratios in boreal biomass burning pollution from previous studies and from the  
 877 POLMIP model simulations analysed in this study. Green: values from plumes of age > 5 days; yellow:  
 878 values from plumes of age <1-5 days. POLMIP model values are classified by age since emission (red:  
 879 aged; blue: young), based on the by the  $\ln([C_3H_8]/[C_2H_6])$  concentration ratio (see text for details).  
 880 Hatched bars indicate average values for each category. Literature values for previous studies are  
 881 based on an updated version of the review of Jaffe and Wigder, (2012).



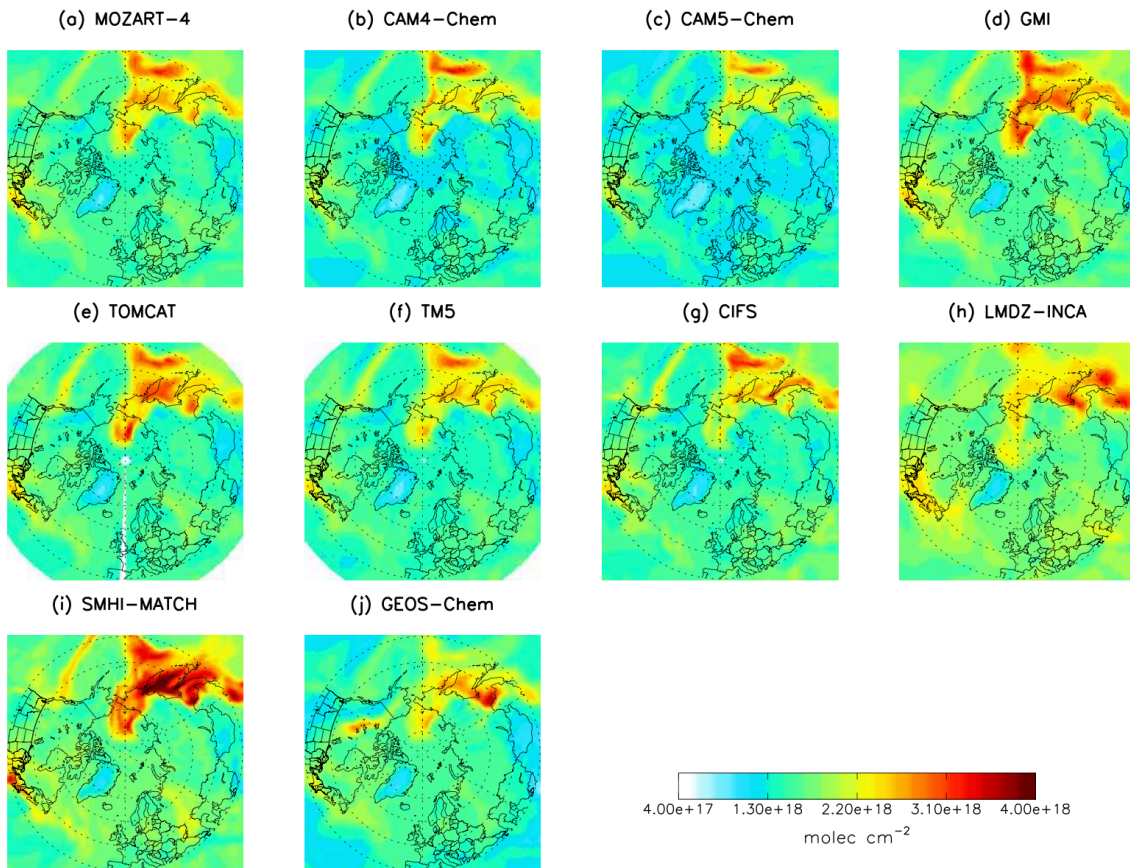
882

883 **Figure 7:** July 2008 PAN/CO relationships for POLMIP models coloured by fire influence. Black: all  
 884 points north of 50N, with 850 hPa > pressure > 250 hPa. Red points show model grid boxes where the  
 885 fire fixed-lifetime CO tracer contributes more than 66% of the total (fire + anthropogenic) tracer  
 886 mixing ratio. Red text gives  $\Delta\text{PAN}/\Delta\text{CO}$  slope values for linear regressions of the red points. GEOS-  
 887 Chem model did not supply fixed-lifetime tracers. Letters in square brackets denote the  
 888 meteorological analysis data used to drive the models - E: ECMWF; G: GEOS-5. Panel (k) shows  
 889 ARCTAS-B aircraft observations with slopes from ECMWF (blue) and GEOS-5 (green) models shown  
 890 for comparison.



891

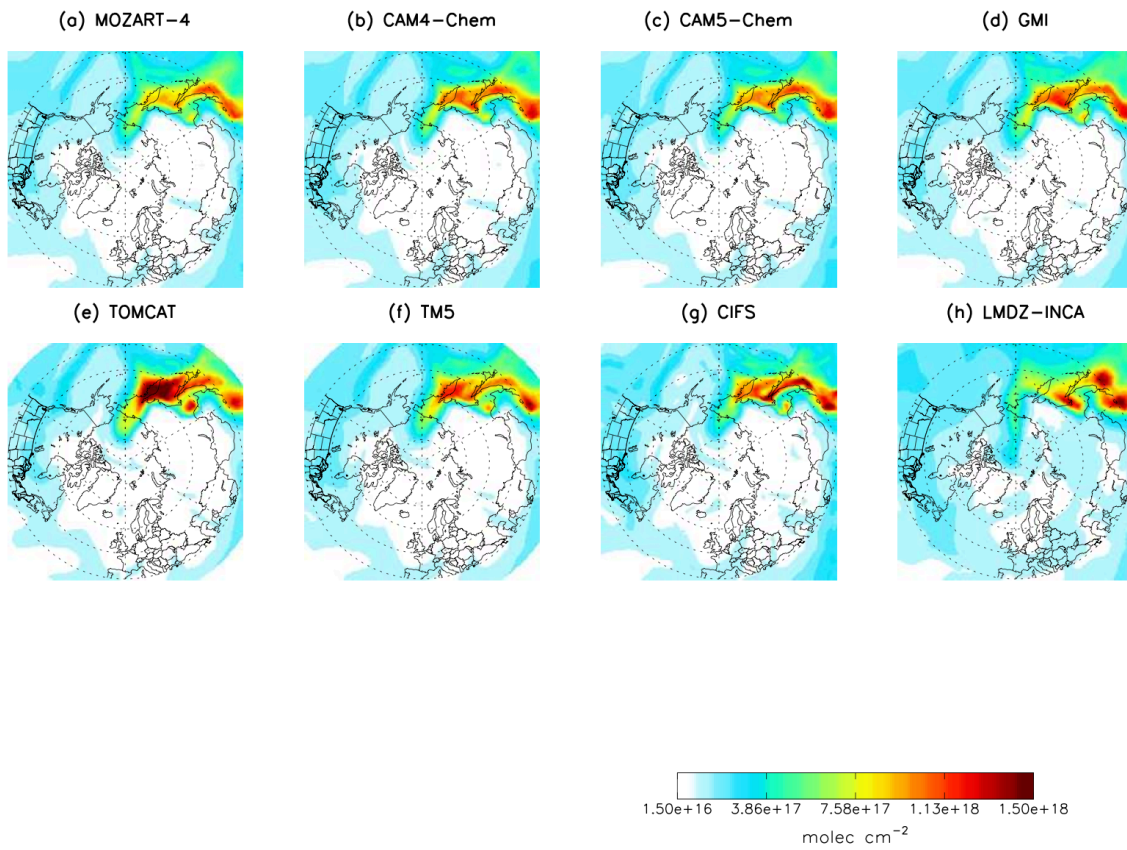
892 **Figure 8:** Zonally-averaged difference between simulated 25-day fixed lifetime CO tracer mixing  
 893 ratios at 900 hPa and 500 hPa in the POLMIP model simulations for (a) spring (MAM) and (b) summer  
 894 (JJA) 2008.



895

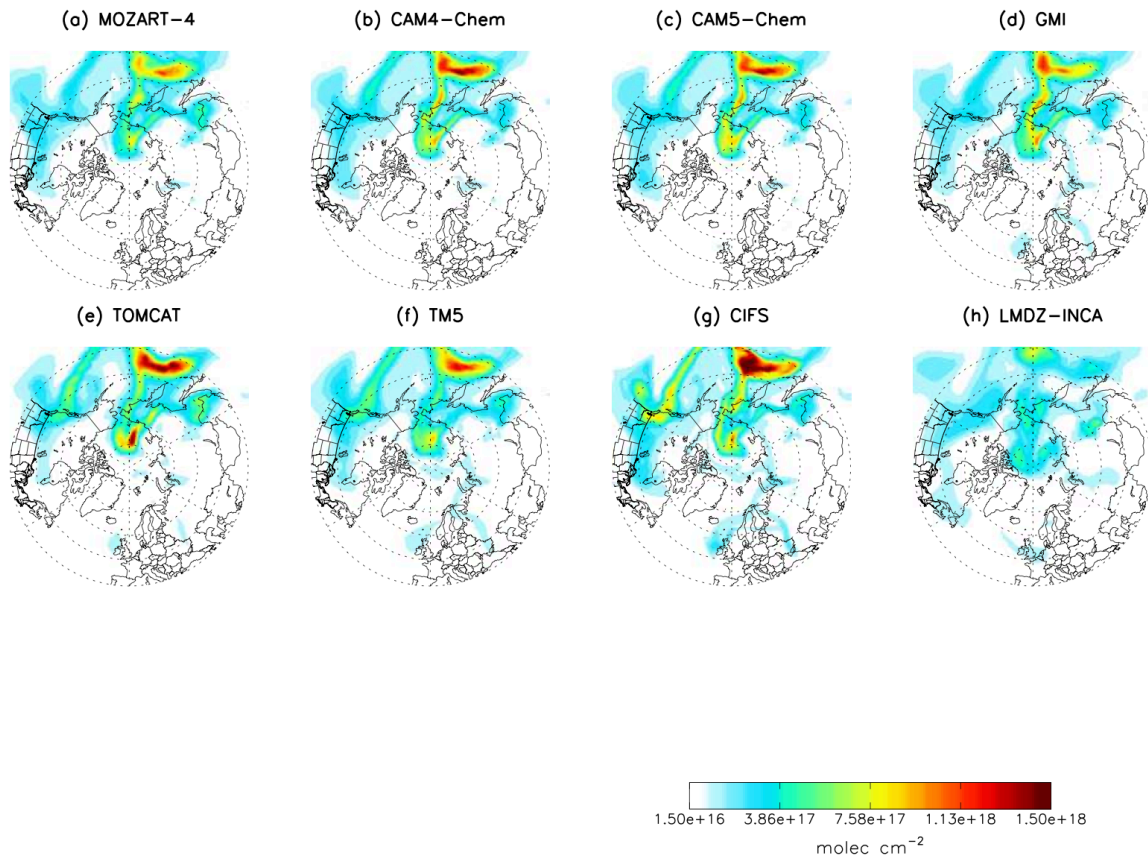
896 **Figure 9:** Total column CO from the POLMIP model simulations at 06UT on 7<sup>th</sup> July 2008.

897



898

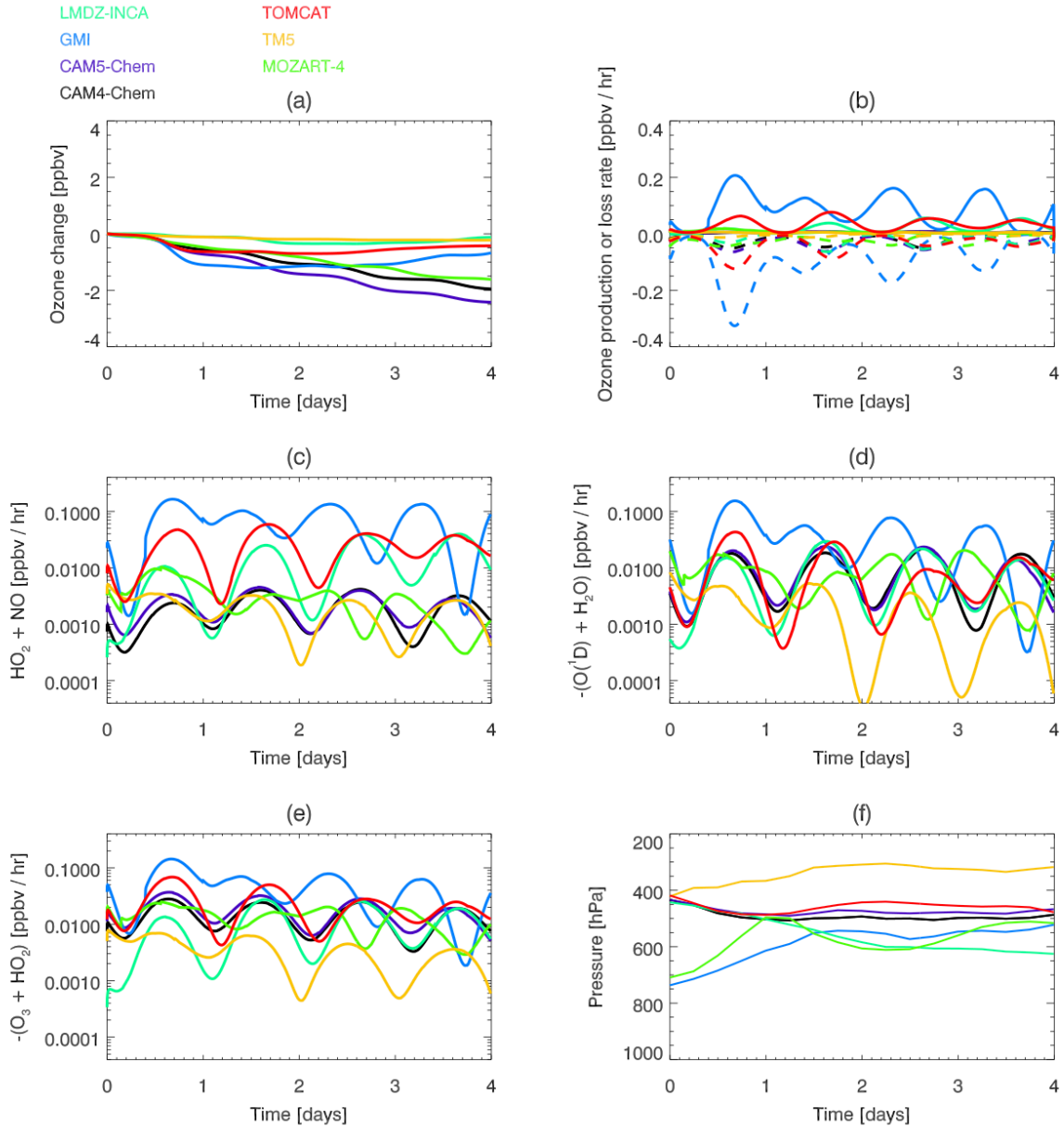
899 **Figure 10:** Total column concentrations of the 25-day fixed-lifetime Asian anthropogenic tracer from  
 900 the POLMIP model simulations at 06UT on 7<sup>th</sup> July 2008.



901

902 **Figure 11:** Total column concentrations of the 25-day fixed-lifetime Asian fire tracer from the POLMIP  
 903 model simulations at 06UT on 7<sup>th</sup> July 2008.

904

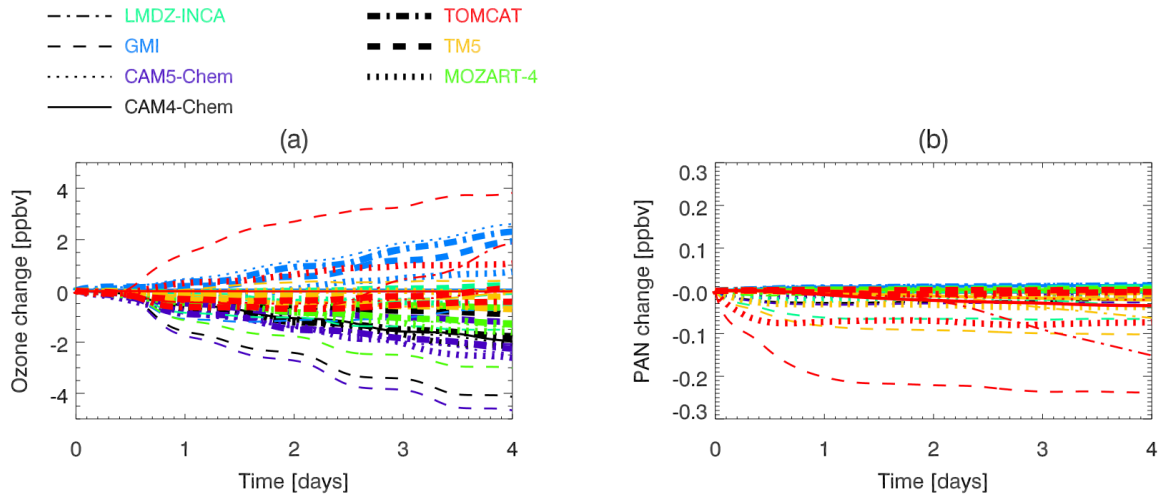


905

906 **Figure 12:** CiTTyCAT Lagrangian box model simulations of fire plume ozone evolution in the Arctic.  
 907 Coloured lines show simulations initialised with chemical composition from each of the POLMIP  
 908 global models at the fire plume maxima locations at 06UT on 7<sup>th</sup> July 2008. (a) Net ozone change  
 909 over the 4-day simulations. (b) Integrated ozone production (solid) and loss (dashed) rates. (c) Rate of  
 910  $\text{HO}_2 + \text{NO}$  ozone production; (d) Rate of  $\text{O}(^1\text{D}) + \text{H}_2\text{O}$  ozone loss; (e) Rate of  $\text{HO}_2 + \text{O}_3$  ozone loss; (f)  
 911 Pressure of forward trajectories from each POLMIP model plume maximum position used for the  
 912 Lagrangian simulations. See text for details of the Lagrangian model simulations.

913

914

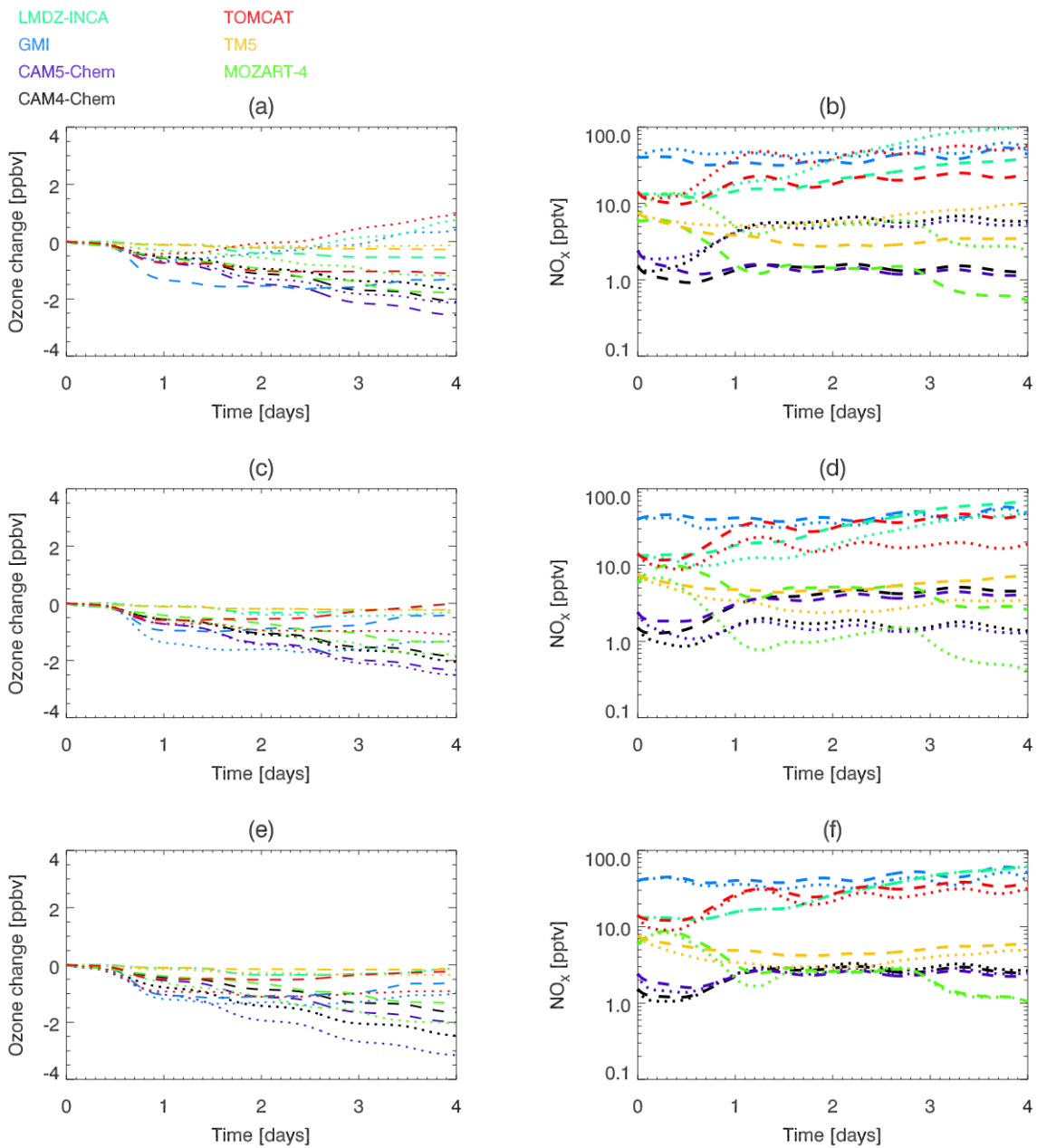


915

916

917 **Figure 13:** Time evolution of fire plume ozone (a) and PAN (b) from CiTTYCAT Lagrangian model  
 918 simulations in which the initial plume concentrations from each of the POLMIP models have been  
 919 used in combination with each of the forward trajectories from the different POLMIP model plume  
 920 positions (shown in Fig. 12f). Different colours correspond to the POLMIP model initial chemical  
 921 conditions and line styles correspond to POLMIP model forward trajectories.

922



923

924

925 **Figure 14:** CiTTyCAT Lagrangian box model simulations showing sensitivity of fire plume ozone and  
 926 NO<sub>x</sub> evolution in the Arctic to initial concentrations of key species. Dotted and dashed lines show  
 927 simulations initialised with 200% and 50% respectively of PAN (a-b), acetone and acetaldehyde (c-d),  
 928 H<sub>2</sub>O<sub>2</sub> and CH<sub>3</sub>OOH (e-f). Ozone change from simulations with un-perturbed initial concentrations are  
 929 shown in Fig. 12a.

930